The influence of sea-ice cover on air-sea gas exchange estimated with radon-222 profiles

Michiel M. Rutgers van der Loeff[1], Nicolas Cassar[2], Marcel Nicolaus[1], Benjamin Rabe[1] and Ingrid Stimac[1]

[1] Alfred Wegener Institute, Helmholtz Centre for Polar and Marine Research, Bremerhaven, Germany

[2] Division of Earth and Ocean Sciences, Nicholas School of the Environment, Duke University, Durham, NC 27708, USA

Abstract

Air-sea gas exchange plays a key role in the cycling of greenhouse and other biogeochemically important gases. Although air-sea gas transfer is expected to change as a consequence of the rapid decline in summer Arctic sea ice cover, little is known about the effect of sea-ice cover on gas exchange fluxes, especially in the marginal ice zone. During the Polarstern expedition ARK-XXVI/3 (TransArc, Aug/Sep 2011) to the central Arctic Ocean, we compared $^{222}Rn/^{226}Ra$ ratios in the upper 50m of 14 ice-covered and 4 ice-free stations. At three of the ice-free stations, we find ^{222}Rn-based gas transfer coefficients in good agreement with expectation based on published relationships between gas transfer and wind speed over open water when accounting for wind history from wind reanalysis data. We hypothesize that the low gas transfer rate at the fourth station results from reduced fetch due to the proximity of the ice edge, or lateral exchange across the front at the ice edge by restratification. No significant radon deficit could be observed at the ice-covered stations. At these stations, the

average gas transfer velocity was less than 0.1 m/d (97.5% confidence), compared to 0.5-2.2 m/d expected for open water. Our results show that air-sea gas exchange in an ice-covered ocean is reduced by at least an order of magnitude compared to open water. In contrast to previous studies, we show that in partially ice-covered regions, gas exchange is lower than expected based on a linear scaling to percent ice cover.

1. Introduction

Air-sea gas exchange is a key aspect of the global cycle of greenhouse gases such as carbon dioxide (CO_2), nitrous oxide (N_2O) and methane (CH_4), as well as other climatically important gases such as dimethylsulfide (DMS). Processes at the ocean surface cause gas saturation to deviate from equilibrium, leading to a net flux (F) driven by the air-sea concentration gradient:

$$F = k(C_{water} - \alpha p_{air}) \qquad (1)$$

where C_{water} is the concentrations of the gas in surface water, p_{air} is the partial pressure of the gas in air, and α is the solubility of the gas in water. The proportionality constant k is called the gas transfer velocity (md^{-1}) and is sometimes presented as k_{660}, a "piston velocity" normalized to a Schmidt number of 660 (the value for CO_2 at 20°C in seawater).

Wind speed exerts a dominant role on gas exchange. The relationship between gas transfer velocity and wind speed has been extensively studied using various methods including bomb-^{14}C oceanic invasion, exchange of ^3He compared to SF_6 tracers, and eddy covariance measurements of CO_2 and DMS in the atmosphere just above the sea surface (Ho et al., 2006; Ho et al., 2011; Nightingale et al., 2000; Sweeney et al., 2007; Wanninkhof, 1992; Wanninkhof and McGillis, 1999). A fourth method is based on the measurement of ^{222}Rn depletion with respect to ^{226}Ra in surface waters. ^{222}Rn is a radioactive noble gas produced through the decay of ^{226}Ra. At depth, ^{222}Rn is at secular equilibrium with the parent isotope. At the surface, the deficit in ^{222}Rn relative to secular equilibrium is proportional to ^{222}Rn loss to the atmosphere integrated over its radioactive life and residence time (Bender et al., 2011; Peng et al., 1979). This method has been applied extensively during the GEOSECS program (Peng et al., 1979). The radon approach harbors uncertainties, including varying mixed layer depth history, inhomogeneous concentration of the parent ^{226}Ra, and assumption of steady state and lateral homogeneity (see Bender et al., 2011; Kromer and Roether, 1983; Liss, 1983; Peng et al., 1979; Roether and Kromer, 1978 for a thorough discussion of the uncertainties associated with the radon approach). Many other factors influence gas transfer velocity, including fetch, surface films, bubbles, rain (Ho et al., 2004), and sea ice (among others, see Wanninkhof et al. (2009) for review). Although the reduction in summer sea ice cover in the Arctic Ocean is expected to alter gas exchange rates (Parmentier et al., 2013), the influence of sea-ice cover on air-sea gas transfer kinetics is poorly constrained. In addition, physical, chemical and biological processes within the sea ice matrix are sources and sinks of various gases, including CO_2 (Dieckmann et al., 2008; Semiletov et al., 2004) and CH_4 (Damm et al., 2010), thereby also influencing the exchange with the atmosphere (see Parmentier et al. (2013) for review).

But apart from these active sources and sinks within the ice, sea ice passively limits gas exchange between atmosphere and water. Poisson and Chen (1987) estimated that the pack ice of the Weddell Sea effectively blocked gas exchange with the atmosphere because very little anthropogenic CO_2 could be found in newly formed Antarctic Bottom Water. Conversely, Fanning and Torres (1991) described gas exchange as only “slightly less than in ice-free seawater” in partially (70-90%) sea ice covered water based on ^{222}Rn measurements over the Barents Sea shelf. They observed large but shallow depletion in summer and small but deep reaching depletion in winter and concluded that despite more complete sea ice cover in winter, the gas transfer velocity varied little between summer and winter due to the presence of fractures or other weaknesses in the ice cover. Fanning and Torres (1991) consequently described sea ice as a 'porous' barrier to the uptake of CO_2. More recently, Loose et al. (2009) found in laboratory experiments that the gas transfer velocity exceeds a linear scaling to percent open water. Loose and Schlosser (2011) later used CFC and ^{3}He data under an ice station in the Weddell Sea to estimate the gas transfer coefficient through nearly complete ice cover. They estimated an average k_{660} of 0.11 m d^{-1} under nearly 100% ice cover, higher than inferred by Poisson and Chen (1987), but much lower than the values found by Fanning and Torres (1991). Based on a 1-D transport model, Loose and Schlosser (2011) also demonstrated that much of the net annual CO_2 flux in the sea ice zone occurs under partially ice-covered conditions, highlighting the importance of better understanding gas fluxes under a wide range of ice conditions. Recently, Kort et al. (2012) observed increased atmospheric CH_4 concentration in regions in close proximity to ice leads and fractional sea ice cover in the Arctic Ocean. Because of the discrepancies and the limited number of observations, there is a large uncertainty in the extent to which the dramatic decline in summer sea ice cover in the Arctic Ocean will cause an increase in gas exchange rates. In this study we investigate the influence of percent sea ice cover on gas exchange in the Arctic Ocean using a $^{222}Rn/^{226}Ra$

disequilibrium methodology similar to the one employed by Fanning and Torres (1991). Parallel detailed shipboard and satellite-based observations of hydrography, wind and sea ice conditions provide a unique background for the interpretation of the radon data. We compare 14 stations in the central Arctic Ocean with 56-100% sea ice cover to 4 stations in the Eurasian Basin that had become ice-free during the weeks prior to our sampling.

2. Sample collection and measurement:

2.1 Location, ice and wind conditions

Water samples were collected during summer of 2011 on the Polarstern expedition ARK XXVI/3 (cruise report Schauer, 2012). The physical oceanography dataset is available from Schauer et al. (2012). Sampling started on a transect from Franz Josef Land towards the North Pole. The first station (201, 13 August 2011), located directly outside the Russian Exclusive Economic Zone (EEZ), was under full sea ice cover. After occupying the last sea ice station on September 19 (Sta 271) we continued southward into the Laptev Sea (Fig. 1). Station coordinates, sampling date and time, as well as wind speed are listed in Table 1.

Sea ice conditions were observed from the vessel's bridge along the entire transect. Hourly observations included, among others, sea ice concentration, sea ice thickness, sea ice type (multi-year and first-year ice), floe size, and melt pond coverage (Schauer, 2012). From this data set (Nicolaus et al., 2012), the sea ice conditions were determined for each station (Table 1). In order to judge the sea ice cover history prior to the sampling, AMSR-2 satellite sea ice concentration data (available from http://www.meereisportal.de) were used at a resolution of 6x6 km. The sea ice concentration of the closest satellite pixel was averaged with its eight neighbors for each day, whereas the center pixel was weighted with a factor of 4 (1/3 of the mean). Sea ice concentrations in the three weeks preceding sampling were weighted according to ^{222}Rn-decay following the approach used by Bender et al. (2011) for wind reanalysis (Table 1). Additional descriptions and photographs of sea ice conditions during the ice stations are available from Nicolaus and Katlein (2013).

Following Bender et al. (2011) we estimated wind history from wind reanalysis data available for locations nearest to each station. We used the ERA interim data of ECMWF with 12-hour and 1.5° resolution because this reanalysis product performs well over the central Arctic Ocean (Jakobson et al., 2012). The effect of wind on gas exchange in the weeks prior to sampling was weighted according to the approach of Bender et al. (2011), which includes the effects of surface ^{222}Rn decay and removal by air-sea exchange (wt2 in Table 2). Because our study shows that ^{222}Rn removal from the water column is slow in ice-covered regions, we also calculated weight factors based on ^{222}Rn decay alone. We consider this weighing procedure (wt1 in Table 2) to be more appropriate for the sea ice covered stations.

2.2 Sampling

At 18 stations, six 30-L Niskin bottles mounted on a special rosette (Multi Water Sampler, Hydrobios Kiel) were closed at 2, 5, 10, 20, 30, and 50m depth. When the ship was in sea ice covered waters, an ice-free working area was maintained next to the ship by the action of bow and stern thrusters, ventilating the upper approximately 8m of the water column with water from under the ice (see discussion below on the potential impact of ship thrusters on ^{222}Rn measurements). 27L of water from these bottles were transferred into evacuated 30-L PVC bottles following the method of Key et al. (1979).

2.3 Analyses

We followed the radon analysis procedure of Mathieu et al. (1988). The original transfer system, designed to transfer the radon by circulation of helium from the 30-L PVC bottles to an activated charcoal column, was not available. We had to rebuild the transfer system on board using the pumps and tubing from a spare Radium Delayed Coincidence Counter (RaDeCC) unit (Moore and Arnold, 1996). This situation may have contributed to higher standard errors than reported in the literature (e.g. Schlosser et al., 1984) and to the relatively high blanks. Blanks, determined by repeatedly analyzing the same water sample, amounted to 1.1±0.3 dpm/100L. One of the four activated charcoal columns did not function properly. The data from that column were discarded, which explains why one out of four data points is missing up to Sta 257. The radon transfer and counting system was calibrated against a ^{226}Ra standard solution (Isotrack, AEA Technology QSA, Product code RAP 10040) obtained from IAEA.

After stripping the radon gas, the samples were drained over columns filled with MnO_2 fibers at flow rates ≤ 1 L min^{-1} to efficiently collect the radium (Moore (1976). Efficiencies of 97±3% were reported for this method by Moore (2008), but the lab intercomparison reported by Charette et al. (2012) yielded average efficiencies of only 87-94%. Our own extraction efficiencies, determined by analyzing two columns filled with MnO_2 fibers in series, were 95-

100%. At the home laboratory, Ra was leached from the fibers (Elsinger et al., 1982), coprecipitated as $BaSO_4$ (Cutter et al., 2010) and ^{226}Ra was measured by gamma spectroscopy using the gamma emission lines at 295, 351, and 609 keV (Moore, 1984). The gamma spectrometer was calibrated against the same IAEA ^{226}Ra standard used for ^{222}Rn calibration.

Precision and accuracy of the $^{222}Rn/^{226}Ra$ activity ratio (AR) was assessed from results at depths where secular equilibrium can be assumed. A depletion is expected primarily in the surface mixed layer, but if there is strong gas exchange and a weak pycnocline, diffusion through the pycnocline might cause some depletion at greater depths as well. The lack of a significant difference in the average $^{222}Rn/^{226}Ra$ AR above and below the strong halocline at sea ice covered stations is indicative of very weak exchange (see discussion below) and makes it highly unlikely that a disequilibrium exists below the pycnocline. The standard deviation of the $^{222}Rn/^{226}Ra$ ratio below the pycnocline in ice-covered stations was 9.7%, resulting from uncertainties in the ^{226}Ra and ^{222}Rn analyses of 8 and 6%, respectively. The average $^{222}Rn/^{226}Ra$ ratio in these samples was 0.982 ± 0.042 (95% confidence interval, CI, n=23), which includes the extraction efficiency of radium on the MnO_2 fibers. All $^{222}Rn/^{226}Ra$ ratios have been normalized with this factor (Table 3). The standard error of mean values (as in Table 2 the mean values of all samples in the mixed layer) is obtained from the standard deviation divided by the square root of the number of observations. The confidence interval of a mean is calculated as the standard error of the mean times the t-value for the indicated level of confidence and degrees of freedom (number of observations-1).

The fraction of Pacific water was estimated from the nutrient composition following Jones et al. (1998), using for waters of Atlantic and Pacific origin the N/P characteristics given by Bauch et al. (2011) and Yamamoto-Kawai et al. (2008), respectively (cf Newton et al., 2013) (Table 3).

3. Results

3.1 Hydrography and mixed layer depth

Just as heat transfer is strongly impeded by the pycnocline at the base of the mixed layer (Toole et al., 2010), ^{222}Rn depletion is expected to be limited to the mixed layer. The mixed layer depth (MLD) was estimated from CTD profiles according to Shaw et al. (2009). In this procedure, MLD is defined as the depth where density increased from its surface value to 20% of the difference between 100-m and surface values. At ice-covered stations (Sta 201-272), the MLD clustered around 20m (Fig. 2).

The average MLD for hydrographic stations 201-285 was 21.5 ± 4.6m (standard deviation). A salinity-driven stratification close to 20m was observed in open water at the end of the expedition (Fig. 3). At Sta 273, just after leaving the sea ice covered region, the procedure of Shaw et al. (2009) yielded a MLD of 34m, but there was a density gradient from 23m downward (Fig. 3). Further south, at Stations 276, 280, and 285, the pycnocline at about 20m became stronger southward with decreasing salinity and increasing temperature of the surface water. We assume an average h_{ML} (MLD) of 21m at all stations. This includes Sta 273 because of the small density gradient at 23m (Fig. 3), which is close to the average MLD, and because no ^{222}Rn depletion was observed below 20m depth (see discussion of the exceptional situation at this station below). Further south at Sta 276, 280 and 285, the homogeneous ^{222}Rn depletion at 2, 5 and 10 but not 20m depth (see below) suggests a MLD of less than 20m. However, the hydrographic profiles (Fig. 3) clearly show that the MLD was mostly between 20 and 22m with only one exceptionally low value of 16m for one cast at Sta 285 (Fig. 2). Apparently, the 20m radon samples were obtained just below the mixed layer. For these stations we have used the same MLD of 21m in our calculations, but we have based the average ^{222}Rn depletion on the values in the upper 15m only.

3.2 ^{222}Rn and ^{226}Ra

^{222}Rn and ^{226}Ra profiles at the 18 stations are presented in Table 3 (data available at http://dx.doi.org/10.1594/PANGAEA.823179). ^{226}Ra is dependent on salinity, uptake by plankton, and on the fraction of water of Pacific origin, which is enriched in ^{226}Ra compared to water of Atlantic origin (Rutgers van der Loeff et al., 2012). In the present study, the correlation of salinity-normalized ^{226}Ra activity $^{226}Ra_{35}$ (dpm/100L) against the Pacific water fraction f_p is given by $^{226}Ra_{35} = 8.83 + 4.54 f_p$ ($R^2 = 0.73$, Fig. 4a). $^{226}Ra_{35}$ is highest at the North Pole station (Sta 218) where the fraction of Pacific water is 71-78% in the upper 30m (Table 3, Fig. 4a,b). In a closed system, without any exchange with the atmosphere, ^{222}Rn should be in secular equilibrium with its parent ^{226}Ra ($^{222}Rn/^{226}Ra$ ratio = 1). We expect this situation below the mixed layer where exchange with the atmosphere should be negligible on the time scale of ^{222}Rn decay. In fact, we did not observe a significant disequilibrium at any depth at all stations with sea ice cover (Fig. 5 left panel). We have no explanation for occasional activity ratios significantly > 1 (Fig. 5 left panel). Similar observations were explained by Fanning and Torres (1991) as resulting from release by sediments, but that process can be excluded because of the large water depths in our study. Ice formation could have rejected Rn and Ra and thus have enhanced their concentrations in the surface water and changed their concentration ratio. During the last part of the expedition, especially after Sept. 4, the temperature fell below the freezing temperature of seawater and ice formation was apparent (Fig. 6, Nicolaus et al., 2012). Using the air temperature recorded on the ship and the freezing degrees days model of Anderson (1961) for the two weeks preceding sampling, we estimate an ice growth of 9.8 cm at Sta 257 and of 10.4 cm at Sta 271. Top et al. (1988) showed in laboratory experiments that the heavier noble gases Ar, Xe, Kr were rejected to 50-60% during ice formation. However, to the best of our knowledge no rejection has been reported for radon. We therefore use extreme values to assess the possible effect of freezing on the derived $^{222}Rn/^{226}Ra$ budget. Even if the frozen layer rejected all Rn but no Ra, the $^{222}Rn/^{226}Ra$ activity ratio would only increase by 0.5%, well within the precision of our technique. This is because the amount of water freezing is small relative to the size of the surface layer, hence not providing enough leverage to influence the water column $^{222}Rn/^{226}Ra$. Surface layer (i.e. 2, 5, and 10m samples) ^{222}Rn depletion was only observed at open-water stations: marginally at the first station after we left the ice (Sta 273) and considerably larger at the other three stations (Fig. 5 right panel). The average $^{222}Rn/^{226}Ra$ AR of all samples shallower than 20m at open-water stations (Sta 276, 280 and 285) was 0.60 ± 0.04 (95% CI, n=9), compared to 1.00 ± 0.04 (95% CI, n=31) at sea ice covered stations (St 201-271).

3.3 Assessing the impact of ship turbulence on MLD and ^{222}Rn measurements

Turbulence associated with ship activity could significantly influence MLD and surface ^{222}Rn measurements. At some stations, mobile ice-floe (away from ship influence) and ship-based CTD observations were compared to assess whether the ship disturbed the MLD. At Sta 209 these procedures agreed well, with an estimated MLD of 15-20m (Schauer, 2012). An Ice-tethered platform (ITP48) yielded a MLD varying between 20-25m during 3.5 days of deployment, a range consistent with the ship-based observations at nearby Sta 245 and 246 (23m and 21m, respectively). These observations confirm that MLD was not significantly affected by the operation of the ship thrusters.

Ship turbulence could alter the ^{222}Rn deficit in surface waters, or mask fine structure patterns in the ^{222}Rn signal. In order to assess the influence of ship turbulence on ^{222}Rn, we conducted additional ^{222}Rn profiles outside the reach of the ship at 6 sea ice covered stations (Sta 212, 218, 222, 227, 230, 235). A hose with a weight was lowered through a hole in the ice and after ample rinsing the water from selected depths was allowed to flow into pre-evacuated 5-L glass jars. Radon was analysed following the same procedure as for the 27-L samples. No samples were collected for ^{226}Ra analysis. Because of the small sample volumes, the errors associated with these measurements were larger than with the 27-L samples. For each depth level we determined the average ^{222}Rn activity. At these 6 stations, no fine structure in radon activities was observed immediately below the ice and no significant difference was observed between samples collected outside the reach of the ship and shipboard collected samples (Fig. 7). These results, along with the secular equilibrium observed in surface waters at the ice stations, suggest that ship turbulence did not influence the ^{222}Rn deficit.

4. Discussion

4.1 Gas exchange as function of wind history

The $^{222}Rn/^{226}Ra$ method is based on calculation of the evasion rate of ^{222}Rn into the atmosphere from measurements of the cumulative depletion of ^{222}Rn with respect to its parent nuclide ^{226}Ra in the surface ocean. The distribution of ^{226}Ra in the ocean was studied in detail during the GEOSECS program in the 1970s because its ~1600-year half-life made it a suitable candidate for tracing ocean circulation. The primary source of ^{226}Ra to the ocean is diffusion from sediments. Radium behaves as a biointermediate element, being consumed but not depleted in productive surface waters. In a closed system, the 3.8-day half-life daughter ^{222}Rn should be in secular equilibrium with ^{226}Ra. In an open system such as the ocean surface, ^{222}Rn gas diffuses into the atmosphere. The rate of change of ^{222}Rn in the surface ocean can be described as:

$$\frac{\partial A_{222Rn}}{\partial t} = \lambda(A_{226Ra} - A_{222Rn}) - P + V \text{ ,} \qquad (2)$$

where A_{226Ra} and A_{222Rn} are the activities of ^{226}Ra and ^{222}Rn, respectively, λ is the decay constant of ^{222}Rn, *P* is the loss of ^{222}Rn by mixing and gas exchange and V is input by advective fluxes. Assuming steady state and negligible advection (V=0) and exchange through the pycnocline, the radon release rate (*F*) can be estimated from *P* integrated over the mixed layer with depth (h_{ML}):

$$F = \int_z P = \lambda(A_{226Ra} - A_{222Rn})h_{ML} \qquad (3)$$

In our study with only gradually changing ice cover and without very strong winds, we do not expect rapid changes in radon inventory, supporting the assumption of steady state. Under transient meteorological conditions ^{222}Rn may change with time, and solving equation (2) for P then requires repeated measurements (Roether and Kromer, 1978). A change in MLD would also have to be taken into account, but we did not observe a deepening of MLD with progressing season (Fig. 2). Equating the gas flux in (1) and (3) neglecting the ^{222}Rn activity in air (Bender et al., 2011) and rearranging, we find

$$k = \lambda\left(\frac{A_{226Ra}}{A_{222Rn}} - 1\right)h_{ML} \qquad (4)$$

where A_{226Ra}/A_{222Rn} is the average activity ratio in the mixed layer (Tables 2,3; Fig. 8). Based on this approach, we find that the average gas transfer velocity was -0.06 ± 0.14 m/d (95% CI) at the 14 ice-covered stations (Sta 201-271), and 2.41 ± 0.42 md^{-1} at the open water stations (277, 280, 285, excluding 273, see below). While negative values of the gas transfer velocity have no physical meaning, our observations imply that the average air-sea gas exchange was less than 0.1 m/d (97.5% certainty) at the ice-covered stations, a reduction by more than one order of magnitude compared to the open water stations. Over the wide range of ice conditions we experienced (% leads, thickness, meltpond coverage, etc., Table 1), the gas exchange rate was consistently low, in clear contrast with the findings of Fanning and Torres (1991). While melt ponds in the second half of the expedition were frozen over (Table 1), they were open at the stations up to Sta 212. During that period, the higher temperatures likely resulted in larger brine volumes and ice permeability (Freitag and Eicken, 2003). The increase in diffusion rates under such conditions may represent a negligible contribution to gas exchange relative to fractures in the ice (Loose et al., 2011).

At open water stations we expect the gas transfer velocity to be related to wind speed *w*:

$$k = 0.074 w^2 \sqrt{\frac{660}{Sc}} \qquad (5)$$

where the Schmidt number for radon (*Sc*) can be calculated as a function of temperature (Wanninkhof, 1992).

The gas transfer velocities calculated with eq. (4) for the open water stations are weakly correlated with instantaneous wind speed (shipboard data, Table 2, not shown). A more appropriate comparison takes into account wind speed history because radon depletion is the cumulative result of exchange over the ^{222}Rn lifetime (Bender et al., 2011).

The weighted wind speeds and corresponding gas transfer velocities are very similar for the four open water stations. For the last three stations 276, 280 and 285, the radon-based velocities are in good agreement with the predictions from Wanninkhof (1992) or Ho et al. (2011), albeit with very few points over a small range of wind speeds (Fig. 9). The measured gas transfer velocity at Sta 273 is low compared to predictions based on wind speed parameterization. We hypothesize that this deviating behaviour is related to the proximity of this station to the ice edge about 2 km away.

4.2 Gas transfer at the ice edge

Station 273 was situated close to the ice edge and had been ice free for three weeks prior to sampling (Table 1, Fig. 10). Several processes could explain the low ^{222}Rn deficit observed at this station: 1) reduced wind fetch due to shelter by the ice, 2) upwelling or downwelling associated with a front along the ice edge and 3) lateral exchange with waters under the ice cover. Gas exchange can be limited by wind fetch (Frew et al., 2004; Jähne et al., 1989; Wanninkhof, 1992; Wanninkhof et al., 2009). The fetch effect on capillary waves is limited to very short distances (of order 10m, Siems, 1980) but the fetch effect on gravity waves and associated air bubble formation can be active on large scales. The fetch effect, as observed near shore for ozone (Fairall et al., 2006) can be expected to be present near sea ice as well. The proximity of Sta 273 to the ice edge just 2km away may have provided shelter from the winds, thereby reducing wind fetch. Wind history was variable with northerly winds followed by rather strong southerlies shortly before we left the ice (more or less parallel to the ice edge, Fig. 10) for three days and weakening over time (Fig. 11). The wave field at Sta 273 could also be modified by reflection at the ice edge (Dierking, W., 2013pers. comm.).

The low ^{222}Rn depletion at this station may also be associated with processes other than reduced air-sea exchange in connection with wave damping due to the proximity of the ice edge. The ice edge constituted a front between the warmer and fresher water to the south and the saltier waters at freezing temperature in the ice-covered stations to the north (Figs 3,12). The wind prior to sampling the station was dominated by north-/southward components (Fig. 11), along the ice edge around Sta 273 (Fig. 10). Under these conditions, wind forcing has been shown to lead to along-ice-edge jets with upwelling and downwelling at the seaward and iceward side of the ice edge, respectively. This type of upwelling occurs on scales of a few kilometers, dependent on the wind velocity, ice drift and the baroclinic Rossby Radius in the upper water column (Fennel and Johannessen, 1998). The deepened mixed layer at this station (Fig. 12) may have resulted from an earlier downwelling event and subsequent advection of surface waters and sea ice. In this respect, we note that the T and S structure in the upper 20m (Fig. 3) showed evidence of lateral mixing across the ice edge. The noticeable density gradient below about 25 m depth suggests that restratification processes due to horizontal density gradients in the mixed layer (Timmermans et al., 2012) may have been active. The balanced Richardson number, as defined by Timmermans et al. (2012), using density derived from profiles at Sta 273 and adjacent XCTD profiles, is around 103. This indicates that baroclinic instability or submesocale eddies could have been at work to restratify the mixed layer at Sta 273. However, lateral advection of the shallower density gradients at the bottom of the mixed layer between Sta 272 and 274 may also lead to a restratification of the upper part of the mixed layer at Sta 273. There is also the possibility that Sta 273 was located within a mesoscale eddy. The scales of such eddies at the bottom of the surface mixed layer are typically around 10 km (e.g.Timmermans et al., 2008), which is not resolved by our observations. Indeed, the internal Rossby Radius associated with submesoscale variability in the surface mixed layer (seeTimmermans and Winsor, 2013), is around 1 km for Sta 273. Higher spatial resolution density profiles would be needed to determine which of these processes is most likely.

4.3 Gas transfer in ice-covered region

While wind speed parameterization is in good agreement with ^{222}Rn-derived gas transfer velocities in open water distant from the ice edge (Fig. 9; Sta 276, 280, 285), the agreement predictably collapses at ice covered stations. Fig. 13 compares the ^{222}Rn-derived gas transfer velocities with the ones predicted from wind history if these stations had been in open water. Wind history was weighted according to ^{222}Rn decay and flushing in open water (wt2) and only decay in ice-covered areas (wt1 in Table 2). ^{222}Rn-based gas transfer velocities at ice-covered stations (Sta 201-271) are statistically indistinguishable from zero. Had these stations been in open water, a wind speed parameterization predicts gas transfer velocities starting above 1.5m d^{-1} at Sta 201, decreasing to just 0.5 m d^{-1} in the calm Beaufort Gyre (Sta 235-239), and increasing to 2-2.5 m d^{-1} in the Laptev Sea. In comparison, we found that the average gas exchange rate based on ^{222}Rn deficit is less than 0.1 m/d for all 14 ice stations (97.5% certainty, Figs. 8,13). This observed negligible gas exchange rate in sea ice covered regions is in close agreement with the study of Loose and Schlosser (2011) while both studies disagree with the results of Fanning and Torres (1991).

If we define the gas transfer efficiency E_T as the ratio between k_{obs}, the gas transfer velocities as observed from ^{222}Rn, and k_{pred}, the velocity predicted from reanalyzed and weighted wind speed history data

$$E_T = {}^{k_{obs}}\!\big/_{k_{pred}} \qquad (6)$$

we find for the 14 ice-covered stations E_T = -0.11 ± 0.19 (95% CI) or E_T < 0.1 (97.5% CI).

4.4 Gas transfer as function of ice cover

The relationship between gas transfer and percent ice cover in the marginal ice zone can have a large impact on calculated seasonal gas fluxes (Loose and Schlosser, 2011). The original approach has been to assume that the relationship of gas exchange with wind speed holds for the open water fraction whereas no exchange takes place through the ice. This led to the assumption of a linear scaling of gas exchange with fraction open water (i.a. used by Takahashi et al., 2009). If we apply such a linear scaling (Fig. 14a) we find that at intermediate ice cover the ^{222}Rn-derived gas exchange rates are low compared to the wind-predicted exchange rate. Indeed, there are reasons to doubt whether such a linear scaling is correct. On one hand, waves, mixing, and turbulence in the open water fraction of a partially ice covered ocean are dramatically different from the situation in the open ocean at the same wind speed (Loose et al., 2014; Loose et al., 2009). On the other hand, although we know from experiments (e.g. Loose et al., 2009) that diffusion through ice is slow, we do not know if gas exchange can be disregarded in the complete surface area that from satellites is counted as ice-covered and that includes meltponds, small leads and thin new ice.

In order to assess the effect of percent ice cover on gas transfer, we plotted E_T against the weighted fraction of open water (Fig. 14b). Because Fanning and Torres (1991) did not report wind data, no comparable radon-based data are available. The figure shows the low gas exchange rate and consequently low E_T at ice edge station 273. Gas transfer efficiencies at the two stations with intermediate fractions of open water (31% at Sta 257 and 44% at Sta 271) are smaller than expected if it scaled linearly with the fraction of open water (Fig. 14b). Advection from waters under more complete ice cover, new ice formation, and/or reduced fetch associated with sea ice may contribute to the reduction in apparent gas exchange efficiency. We note that Fig. 14 does not take into account the relative motions of sea ice and surface waters over the weighting period.

It is difficult to reconstruct the true % sea ice cover experienced by a given water column over a period of time equivalent to the radon lifetime. From general wind drift data (Hakkinen et al., 2008) and the displacement of the ice edge during our cruise (Fig. 10) we estimate that the wind drift of the sea ice is on the order of 5 cm/s. The associated drift of surface water is slower and declines rapidly down to the Ekman depth (~20m) (Hunkins, 1966). We estimate that the velocity of the bulk of the mixed layer is about 0.5 cm/s (cf. Yang, 2006, their equations 3-5). Because floes were on average less than 500m in size in the week before sampling stations 257 and 271 (Nicolaus et al., 2012), the bulk of the mixed layer in the marginal ice zone likely experienced alternating floes and leads conditions integrated over the radioactive lifetime of radon. We therefore expect the radon depletion to represent an average gas exchange rate over varying % ice cover in a radius of approximately ~20 km (3.5 grids in Fig. 10).

New sea ice formation occurred from approximately 4 Sept onwards (Fig 6). In the interpretation of satellite data, the first stages of ice formation, frazil and grease ice, would not be distinguished from open water. These ice types were not abundant according to the observations from the bridge (Nicolaus et al., 2012). Nevertheless, it is possible that beginning ice formation would have reduced the available ice-free surface area compared to our calculation based on weighted satellite data. The extent to which ice undetectable from satellites could bias satellite based parameterizations of the influence ice on gas exchange (Loose et al., 2014) is unclear.

Loose et al. (2009) predicted based on laboratory experiments that gas exchange in partially ice-covered regions should be more than expected from a linear relationship with ice cover because of the influence of turbulence below the ice on diffusion through the ice pack. Our observations show that gas exchange in the partially ice-covered region we studied is in fact less than expected from a linear relationship with ice cover, potentially due to the influence of reduced wind fetch.

In light of our new observations, and considering that wave mean square slope may be a better predictor of gas transfer velocity than wind speed (Frew et al., 2004), future studies should incorporate high resolution satellite or shipboard observations of surface roughness and mean square slope near the ice edge or in large leads coupled with heat flux measurements (Frew et al., 2004; Jähne et al., 1989).

5. Conclusions

In open water at large distance (>70km) from the ice edge, gas transfer velocities determined with ^{222}Rn were in good agreement with velocities predicted based on a wind speed parameterization (Ho et al., 2011; Wanninkhof, 1992), taking into account wind history. The latter was based on a reanalysis dataproduct using weighting factors calculated following Bender et al. (2011).

In ice-covered regions, there is no indication of a ^{222}Rn-depleted layer at the surface. Hence, over a wide range of ice-covered conditions, air-sea gas exchange was reduced by at least one order of magnitude compared to the open water stations, in agreement with observations made by Loose et al. (2011).

Our observations suggest that reduced wind fetch due to sea ice cover limits gas exchange rate near the ice edge and in partially ice-covered regions, opposing the enhancement of gas exchange associated with turbulence below the ice described by Loose et al. (2009) under laboratory settings. If the relative strength of these processes varies by region or over time, the net effect may be a gas exchange rate greater or less than predicted based on a linear correction to percent sea ice cover.

The relationship between ice cover and gas exchange in partially ice covered regions can have a large effect on calculated annual CO_2 fluxes (Loose and Schlosser, 2011). In contrast to earlier findings from $^{222}Rn/^{226}Ra$ data or laboratory experiments, our study shows that gas exchange can be smaller than predicted if it scaled linearly with ice cover in partially ice-covered areas exposed to wind.

Acknowledgments

We thank captain Schwarze and his crew, chief scientist Ursula Schauer and the participants of ARK-XXVI/3 (TransArc) for their support during the expedition. Daniel Scholz helped with sampling, Kai-Uwe Ludwichowski performed the nutrient analyses, Stephan Frickenhaus gave statistical advice, Frank Kauker helped with the wind reanalysis, and Jölund Asseng with plots of ice cover. We gratefully acknowledge very constructive comments of Peter Schlosser, Brice Loose and an anonymous reviewer. N. C. was partly supported by an Alfred P. Sloan Fellowship. The ^{222}Rn and ^{226}Ra data presented here are available at PANGAEA (http://dx.doi.org/10.1594/PANGAEA.823179).

References

Anderson, D.L., 1961. Growth rate of sea ice. Journal of Glaciology 3, 1170-1172.

Bauch, D., Rutgers van der Loeff, M., Andersen, N., Bakker, K., Torres-Valdes, S., Abrahamsen, P., 2011. Origin of freshwater and polynya water in the Arctic Ocean halocline in 2007. Prog. Oceanogr. 91, 482-495.

Bender, M.L., Kinter, S., Cassar, N., Wanninkhof, R., 2011. Evaluating gas transfer velocity parameterizations using upper ocean radon distributions. Journal of Geophysical Research 116, C02010.

Charette, M.A., Dulaiova, H., Gonneea, M.E., Henderson, P.B., Moore, W.S., Scholten, J.C., Pham, M.K., 2012. GEOTRACES radium isotopes interlaboratory comparison experiment. Limnology Oceanography Methods 10, 451-463.

Cutter, G., Andersson, P., Codispoti, L., Croot, P., Francois, R., Lohan, M., Obata, H., Rutgers van der Loeff, M., 2010. Sampling and Sample-handling Protocols for GEOTRACES Cruises - version 1. GEOTRACES, p. 98pp.

Damm, E., Helmke, E., Thoms, S., Schauer, U., Nöthig, E., Bakker, K., Kiene, R.P., 2010. Methane production in aerobic oligotrophic surface water in the central Arctic Ocean. Biogeosciences 7, 1099-1108.

Dieckmann, G.S., Nehrke, G., Papadimitriou, S., Göttlicher, J., Steininger, R., Kennedy, H., Wolf-Gladrow, D., Thomas, D.N., 2008. Calcium carbonate as ikaite crystals in Antarctic sea ice. Geophys. Res. Lett. 35.

Elsinger, R.J., King, P.T., Moore, W.S., 1982. Radium-224 in natural waters measured by g ray spectrometry. Anal. Chim. Acta 144, 277-281.

Fairall, C.W., Bariteau, L., Grachev, A.A., Hill, R.J., Wolfe, D.E., Brewer, W.A., Tucker, S.C., Hare, J.E., Angevine, W.M., 2006. Turbulent bulk transfer coefficients and ozone deposition velocity in the International Consortium for Atmospheric Research into Transport and Transformation. Journal of Geophysical Research: Atmospheres 111, D23S20.

Fanning, K.A., Torres, L.M., 1991. ^{222}Rn and ^{226}Ra: indicators of sea-ice effects on air-sea gas exchange. Polar Research 10, 51-58.

Fennel, W., Johannessen, O.M., 1998. Wind forced oceanic responses near ice edges revisited. Journal of Marine Systems 14, 57-79.

Freitag, J., Eicken, H., 2003. Meltwater circulation and permeability of Arctic summer sea ice derived from hydrological field experiments. JOURNAL OF GLACIOLOGY 49, 349-358.

Frew, N.M., Bock, E.J., Schimpf, U., Hara, T., Haußecker, H., Edson, J.B., McGillis, W.R., Nelson, R.K., McKenna, S.P., Uz4, B.M., Jähne, B., 2004. Air-sea gas transfer: Its dependence on wind stress, small-scale roughness, and surface films. Journal of Geophysical Research 109.

Hakkinen, S., Proshutinsky, A., Ashik, I., 2008. Sea ice drift in the Arctic since the 1950s. Geophys. Res. Letters 35, L19704.

Ho, D.T., Law, C.S., Smith, M.J., Schlosser, P., Harvey, M., Hill, P., 2006. Measurements of air-sea gas exchange at high wind speeds in the Southern Ocean: Implications for global parameterizations. Geophys. Res. Lett. 33, L16611, doi:16610.11029/12006GL026817.

Ho, D.T., Wanninkhof, R., Schlosser, P., Ullman, D.S., Hebert, D., Sullivan, K.F., 2011. Toward a universal relationship between wind speed and gas exchange: Gas transfer velocities measured with 3He/SF6 during the Southern Ocean Gas Exchange Experiment. Journal of Geophysical Research: Oceans 116, C00F04.

Ho, D.T., Zappa, C.J., McGillis, W.R., Bliven, L.F., Ward, B., Dacey, J.W.H., Schlosser, P., Hendricks, M.B., 2004. Influence of rain on air-sea gas exchange: Lessons from a model ocean. J. Geophys. Res. 109, C08S18, doi:10.1029/2003JC001806.

Hunkins, K., 1966. Ekman drift currents in the Arctic Ocean. Deep Sea Research and Oceanographic Abstracts 13, 607-620.

Jähne, B., Libner, P., Fischer, R., Billen, T., Plate, E.J., 1989. Investigating the transfer processes across the free aqueous viscous boundary layer by the controlled flux method. Tellus B 41B, 177-195.

Jakobson, E., Vihma, T., Palo, T., Jakobson, L., Keernik, H., Jaagus, J., 2012. Validation of atmospheric reanalyses over the central Arctic Ocean. Geophys. Res. Letters 39, L10802, doi:10810.11029/12012GL051591.

Jones, E.P., Anderson, L.G., Swift, J.H., 1998. Distribution of Atlantic and Pacific waters in the upper Arctic Ocean: Implications for curculation. Geophys. Res. Lett. 25, 765-768.

Key, R.M., Brewer, R.L., Stockwell, J.H., Guinasso, N.L., Schink, D.R., 1979. Some improved techniques for measuring radon and radium in marine sediments and in seawater. Mar. Chem. 7, 251-264.

Kort, E.A., Wofsy, S.C., Daube, B.C., Diao, M., Elkins, J.W., Gao, R.S., Hintsa, E.J., Hurst, D.F., Jimenez, R., Moore, F.L., Spackman, J.R., Zondlo, M.A., 2012. Atmospheric observations of Arctic Ocean methane emissions up to 82° north. Nature Geosci 5, 318-321.

Kromer, B., Roether, W., 1983. Field measurements of air-sea gas exchange by the radon deficit method during JASIN 1978 and FGGE 1979. Meteor Forschungsergebnisse A/B24, 55-76.

Liss, P.S., 1983. Gas transfer: Experiments and geochemical implications., in: Liss, P.S., Slinn, W.G.N. (Eds.), Air-Sea Exchange of gases and particles. D. Reidel, Dordrecht, pp. 241-298.

Loose, B., McGillis, W.R., Perovich, D., Zappa, C.J., Schlosser, P., 2014. A parameter model of gas exchange for the seasonal sea ice zone. Ocean Sci. 10, 17-28.

Loose, B., McGillis, W.R., Schlosser, P., Perovich, D., Takahashi, T., 2009. Effects of freezing, growth, and ice cover on gas transport processes in laboratory seawater experiments. Geophys. Res. Letters 36, L05603, doi:05610.01029/02008GL036318.

Loose, B., Schlosser, P., 2011. Sea ice and its effect on CO2 flux between the atmosphere and the Southern Ocean interior. Journal of Geophysical Research 116, C11019, doi:11010.11029/12010JC006509.

Loose, B., Schlosser, P., Perovich, D., Ringelberg, D., Ho, D.T., Takahashi, T., Richter-Menge, J., Reynolds, C.M., McGillis, W.R., Tison, J.-L., 2011. Gas diffusion through columnar laboratory sea ice: implications for mixed-layer ventilation of CO2 in the seasonal ice zone. Tellus 63B, 23-39.

Mathieu, G.G., Biscaye, P.E., Lupton, R.A., Hammond, D.E., 1988. System for measurement of 222Rn at low levels in natural waters. Health Physics 55, 989-992.

Moore, W.S., 1976. Sampling 228Ra in the deep ocean. Deep-Sea Res. 23, 647-651.

Moore, W.S., 1984. Radium isotope measurements using germanium detectors. Nuclear Instruments and Methods in Physics Research 223, 407-411.

Moore, W.S., 2008. Fifteen years experience in measuring ^{224}Ra and ^{223}Ra by delayed coincidence counting. Mar. Chem. 109, 188-197.

Moore, W.S., Arnold, R., 1996. Measurement of ^{223}Ra and ^{224}Ra in coastal waters using a delayed coincidence counter. J. Geophys. Res. 101, 1321-1329.

Newton, R., Schlosser, P., Mortlock, R., Swift, J., MacDonald, R., 2013. Canadian Basin freshwater sources and changes: Results from the 2005 Arctic Ocean Section. Journal of Geophysical Research: Oceans 118, 2133-2154.

Nicolaus, M., Katlein, C., 2013. Mapping radiation transfer through sea ice using a remotely operated vehicle (ROV). The Cryosphere 7, 763-777.

Nicolaus, M., Katlein, C., Maslanik, J.A., Hendricks, S., 2012. Sea ice conditions during the POLARSTERN cruise ARK-XXVI/3 (TransArc) in 2011. doi:10.1594/PANGAEA.803312.

Nightingale, P.D., Law, C.S., Watson, A.J., Liss, P.S., Liddicoat, M., Boutin, J., Upstill-Goddard, R.C., 2000. In situ evaluation of air-sea gas exchange parameterizations using novel conservative and volatile tracers. Global Biogeochem. Cycles 14, 373-387.

Parmentier, F.-J.W., Christensen, T.R., Sorensen, L.L., Rysgaard, S., McGuire, A.D., Miller, P.A., Walker, D.A., 2013. The impact of lower sea-ice extent on Arctic greenhouse-gas exchange. Nature Clim. Change 3, 195-202.

Peng, T.-H., Broecker, W.S., Mathieu, G.G., Li, Y.-H., Bainbridge, A.E., 1979. Radon evasion rates in the Atlantic and Pacific Oceans as determined during the Geosecs Program. J. Geophys. Res. 84, 2471-2486.

Poisson, A., Chen, C.-T.A., 1987. Why is there so little anthropogenic CO2 in the Antarctic Bottom Water? Deep-Sea Res. 34, 1255-1275.

Roether, W., Kromer, B., 1978. Field determination of air-sea gas exchange by continuous measurement of radon-222. Pure and applied geophysics 116, 476-485.

Rutgers van der Loeff, M.M., Cai, P., Stimac, I., Bauch, D., Hanfland, C., Roeske, T., Bradley Moran, S., 2012. Shelf-basin exchange times of Arctic surface waters estimated from ^{228}Th/^{228}Ra disequilibrium. Journal of Geophysical Research - Oceans 117, C03024, doi:03010.01029/02011JC007478.

Schauer, U., 2012. The expedition of the research vessel "Polarstern" to the Arctic in 2011 (ARK-XXVI/3 - TransArc). Reports on polar and marine research 649, 205 pp.

Schauer, U., Rabe, B., Wisotzki, A., 2012. Physical oceanography during POLARSTERN cruise ARK-XXVI/3. doi:10.1594/PANGAEA.774181, Alfred Wegener Institute, Helmholtz Center for Polar and Marine Research, Bremerhaven.

Schlosser, P., Rhein, M., Roether, W., Kromer, B., 1984. High-precision measurement of oceanic 226Ra. Mar. Chem. 15, 203-216.

Semiletov, I., Makshtas, A., Akasofu, S.-I., Andreas, E.L., 2004. Atmospheric CO2 balance: The role of Arctic sea ice. Geophys. Res. Letters 31, L05121, doi:05110.01029/02003GL017996.
Shaw, W.J., Stanton, T.P., McPhee, M.G., Morison, J.H., Martinson, D.G., 2009. Role of the upper ocean in the energy budget of Arctic sea ice during SHEBA. Journal of Geophysical Research: Oceans 114, C06012, doi:06010.01029/02008jc004991.
Siems, W., 1980. Modeluntersuchungen zur Verdunstung und zum Gasaustauch zwischen Wasser und Luft: Der Einfluss von Wellen und Oberflächenverunreinigungen. Univ. of Hamburg, p. 241.
Sweeney, C., Gloor, E., Jacobson, A.R., Key, R.M., McKinley, G., Sarmiento, J.L., Wanninkhof, R., 2007. Constraining global air-sea gas exchange for CO_2 with recent bomb ^{14}C measurements. Global Biogeochem. Cycles 21, GB2015, doi:2010.1029/2006GB002784.
Takahashi, T., Sutherland, S.C., Wanninkhof, R., Sweeney, C., Feely, R.A., Chipman, D.W., Hales, B., Friederich, G., Chavez, F., Sabine, C., Watson, A., Bakker, D.C.E., Schuster, U., Metzl, N., Yoshikawa-Inoue, H., Ishii, M., Midorikawa, T., Nojiri, Y., Körtzinger, A., Steinhoff, T., Hoppema, M., Olafsson, J., Arnarson, T.S., Tilbrook, B., Johannessen, T., Olsen, A., Bellerby, R., Wong, C.S., Delille, B., Bates, N.R., de Baar, H.J.W., 2009. Climatological mean and decadal change in surface ocean pCO2, and net sea–air CO2 flux over the global oceans. Deep Sea Research Part II: Topical Studies in Oceanography 56, 554-577.
Timmermans, M.-L., Cole, S., Toole, J., 2012. Horizontal Density Structure and Restratification of the Arctic Ocean Surface Layer. Journal of Physical Oceanography 42, 659-668.
Timmermans, M.-L., Winsor, P., 2013. Scales of horizontal density structure in the Chukchi Sea surface layer. Continental Shelf Research 52, 39-45.
Timmermans, M.L., Toole, J., Proshutinsky, A., Krishfield, R., Plueddemann, A., 2008. Eddies in the Canada Basin, Arctic Ocean, Observed from Ice-Tethered Profilers. Journal of Physical Oceanography 38, 133-145.
Toole, J.M., Timmermans, M.L., Perovich, D.K., Krishfield, R.A., Proshutinsky, A., Richter-Menge, J.A., 2010. Influences of the ocean surface mixed layer and thermohaline stratification on Arctic Sea ice in the central Canada Basin. Journal of Geophysical Research: Oceans 115, C10018, doi:10010.11029/12009jc005660.
Top, Z., Martin, S., Becker, P., 1988. A laboratory study of dissolved noble gas anomaly due to ice formation. Geophys. Res. Letters 15, 796-799.
Wanninkhof, R., 1992. Relationship between gas exchange and wind speed over the ocean. J. Geophys. Res. 97, 7373-7381.
Wanninkhof, R., Asher, W.E., Ho, D.T., Sweeney, C., McGillis, W.R., 2009. Advances in Quantifying Air-Sea Gas Exchange and Environmental Forcing. Annual Review of Marine Science 1, 213-244.
Wanninkhof, R., McGillis, W., 1999. A cubic relationship between air-sea CO2 exchange and wind speed. Geophys. Res. Lett. 26, 291-301.
Yamamoto-Kawai, M., McLaughlin, F.A., Carmack, E.C., Nishino, S., Shimada, K., 2008. Freshwater budget of the Canada Basin, Arctic Ocean, from salinity, $\delta^{18}O$, and nutrients. Journal of Geophysical Research 113, C01007, doi:01010.01029/02006JC003858.
Yang, J., 2006. The Seasonal Variability of the Arctic Ocean Ekman Transport and Its Role in the Mixed Layer Heat and Salt Fluxes. Journal of Climate 19, 5366-5387.

Table 1. Station time and position, and ice cover from ice observations on the bridge (extracted from doi:10.1594/PANGAEA.803312) and from satellite observations (from http://iup.physik.uni-bremen.de), the latter weighted taking into account ice history over the decay life of ^{222}Rn, ice type (FYI=First Year Ice; MYI=Multi Year Ice, X=no ice), ice thickness (cm) and melt pond fraction.

Station	**Date**	**Time**	**Latitude**	**Longitude**	**Ice cover bridge**	**weighted ice cover**	**Ice type**	**Ice thickness**	**Melt pond fraction**

201	13-08-11	18:48	85° 31,17' N	59° 40,95' E	0.9	0.96	FYI	70-120	0.5
205	15-08-11	15:01	86° 19,72' N	59° 17,37' E	1.0	0.96	MYI	200-300	0.3
209	17-08-11	19:31	86° 58,93' N	58° 58,49' E	1.0	0.94	FYI/MYI	90-300	0.3
212	19-08-11	22:01	88° 1,38' N	59° 26,36' E	1.0	0.94	FYI	70-80	0.4
218	22-08-11	13:16	89° 57,92' N	130° 24,64' E	1.0	1.00*	FYI/MYI	90-250	0.4**
222	26-08-11	11:54	88° 44,46' N	128° 19,41' W	1.0	1.00*	FYI	100-120	0.4**
227	29-08-11	11:28	86° 51,69' N	155° 5,86' W	1.0	0.98	FYI	150	0.35**
230	31-08-11	20:06	85° 3,70' N	137° 16,93' W	1.0	0.98	MYI/FYI	120-250	0.25**
235	02-09-11	23:12	83° 1,63' N	130° 1,49' W	1.0	1.00	FYI/MYI	120-200	0.4**
239	05-09-11	23:58	84° 4,43' N	164° 12,94' W	1.0	0.99	MYI/FYI	70-200	0.25**
245	09-09-11	07:49	84° 48,41' N	166° 25,08' E	1.0	0.99	FYI	60-120	0.1**
250	11-09-11	11:41	84° 22,71' N	139° 52,80' E	0.9	0.96	FYI	50-80	0.4**
257	13-09-11	18:01	83° 20,32' N	124° 52,77' E	0.8	0.69	FYI	40-60	0.2**
271	19-09-11	04:37	82° 9,87' N	119° 10,95' E	0.8	0.56	FYI	30-60	
273	19-09-11	21:15	81° 21,49' N	120° 47,80' E	0.0	0.00	X	X	
276	20-09-11	06:46	80° 38,59' N	121° 19,93' E	0.0	0.00	X	X	
280	21-09-11	06:50	79° 8,87' N	124° 6,56' E	0.0	0.00	X	X	
285	22-09-11	13:39	78° 29,61' N	125° 47,05' E	0.0	0.00	X	X	

* : no satellite data near North Pole; bridge observations at time of sampling used instead.

**:frozen surface

Table 2.

Average $^{222}Rn/^{226}Ra$ in surface mixed layer (21m) and derived gas transfer velocity k, compared with wind (m/s) as measured on board (ship), wind reanalysis during sampling (inst.) and weighted according to ^{222}Rn decay (wt1) and decay plus MLD flushing (wt2) and corresponding values of the gas transfer velocity following Wanninkhof (1992). Last column gives (meteorological) wind direction of wind reanalysis with ^{222}Rn decay weighting.

			ship	wind reanalysis						
Station	Rn/Ra	k(^{222}Rn)	wind	inst.	wt1*	wt2**	kship	kwt1	kwt2	Dir***
	av MLD	m/d	m/s	m/s	m/s	m/s	m/d	m/d	m/d	degr.
201	0.92 ± 0.10	0.34 ± 0.47	7	6.13	6.94	7.27	1.59	1.57	1.72	118
205	0.96 ± 0.07	0.16 ± 0.28	7	4.47	6.23	5.97	1.59	1.26	1.16	128
209	1.00 ± 0.07	0.01 ± 0.28	10	4.88	6.19	6.02	3.25	1.25	1.18	173
212	1.04 ± 0.07	-0.14 ± 0.24	3	3.56	5.67	5.38	0.29	1.05	0.94	187
218	0.97 ± 0.05	0.13 ± 0.22	9	6.29	5.30	5.17	2.64	0.91	0.87	305
222	1.15 ± 0.07	-0.50 ± 0.21	0	1.95	5.92	5.78	0.00	1.14	1.09	123
227	1.02 ± 0.07	-0.09 ± 0.24	1	2.42	5.28	4.77	0.03	0.91	0.74	60
230	1.09 ± 0.07	-0.31 ± 0.21	7	4.30	4.80	4.34	1.59	0.75	0.61	100
235	1.15 ± 0.07	-0.51 ± 0.21	4	3.39	3.90	3.64	0.52	0.50	0.43	80
239	0.97 ± 0.06	0.12 ± 0.23	4	4.88	3.90	3.64	0.52	0.50	0.43	80
245	1.06 ± 0.07	-0.21 ± 0.25	5	2.28	5.52	5.67	0.81	0.99	1.04	285
250	1.02 ± 0.08	-0.06 ± 0.28	12	8.98	8.24	9.58	4.69	2.21	2.99	337
257	0.98 ± 0.07	0.08 ± 0.28	11	5.26	6.98	6.52	3.94	1.59	1.38	341
271	0.97 ± 0.06	0.11 ± 0.25	8	3.77	7.82	7.78	2.08	1.99	1.97	208
273	0.87 ± 0.05	0.56 ± 0.27	6	2.83	7.89	7.66	1.17	2.03	1.91	214
276	0.63 ± 0.04	2.27 ± 0.42	7	3.98	8.36	8.52	1.59	2.27	2.36	248
280	0.62 ± 0.04	2.35 ± 0.44	10	9.04	8.36	8.38	3.25	2.27	2.29	248
285	0.59 ± 0.04	2.60 ± 0.45	11	7.43	8.28	8.03	3.94	2.23	2.10	302

*) weighted with ^{222}Rn decay only

**) weighted with ^{222}Rn decay and MLD flushing

***) meteorological wind direction for reanalysis with ^{222}Rn-decay weighting.

Table 3. ^{222}Rn, ^{226}Ra, normalized $^{222}Rn/^{226}Ra$ with SE, salinity, ^{226}Ra normalized to 35‰ compared with nutrient data at nearest sampled depth with CTD/Rosette: phosphate, nitrate+nitrite, and the computed fraction of Pacific water.

Station	**depth**	**^{222}Rn**	**^{226}Ra**	**^{222}Rn/^{226}Ra***	**Salinity**	**^{226}Ra$_{35}$**	**CTDdepth**	**PO$_4$**	**NO$_{2+3}$**	**f$_{Pac}$****
	(m)	(dpm/100L)	(dpm/100L)			(dpm/100L)	(m)	(µM)	(µM)	
201	10	7.51 ± 0.40	8.32 ± 0.81	0.92 ± 0.10	33.24	8.76	10	0.16	3.16	-0.20
201	30	7.09 ± 0.38	8.95 ± 0.91	0.81 ± 0.09	34.01	9.21	25	0.18	3.92	-0.23
201	40	7.56 ± 0.40	8.67 ± 0.85	0.89 ± 0.10	34.10	8.89				
201	50	8.37 ± 0.43	8.05 ± 0.81	1.06 ± 0.12		8.23				
205	1	7.83 ± 0.41	8.83 ± 0.82	0.90 ± 0.10	32.90	9.39				
205	7	7.69 ± 0.42	8.49 ± 0.80	0.92 ± 0.10	33.19	8.95	10	0.11	0.71	-0.07
205	17	8.54 ± 0.46	8.28 ± 0.91	1.05 ± 0.13	33.80	8.58				
205	27	9.29 ± 0.50	7.79 ± 0.92	1.22 ± 0.16	34.05	8.00	25	0.19	1.93	-0.05
209	2	6.32 ± 0.34	8.35 ± 0.84	0.77 ± 0.09	32.80	8.91				
209	5	7.82 ± 0.42	7.89 ± 0.90	1.01 ± 0.13	32.90	8.39	5	0.22	1.23	0.05
209	10	9.10 ± 0.48	7.64 ± 0.84	1.21 ± 0.15	32.85	8.14	10	0.23	1.21	0.05
212	2	9.17 ± 0.48	8.13 ± 0.82	1.15 ± 0.13	32.20	8.84				
212	5	8.92 ± 0.47	10.20 ± 0.84	0.89 ± 0.09	32.30	11.05	5	0.41	2.48	0.20
212	20	10.27 ± 0.53	9.70 ± 0.95	1.08 ± 0.12	33.20	10.22	25	0.49	3.27	0.25
212	30	8.66 ± 0.45	9.90 ± 0.82	0.89 ± 0.09	33.30	10.41	25	0.49	3.27	0.25
212	50	9.21 ± 0.48	9.13 ± 0.86	1.03 ± 0.11	33.30	9.59	50	0.56	5.85	0.13
218	5	12.31 ± 0.64	12.30 ± 0.88	1.02 ± 0.09	32.00	13.45	5	0.88	3.26	0.78
218	10	12.05 ± 0.62	11.83 ± 0.89	1.04 ± 0.09	31.95	12.96	10	0.96	4.63	0.76
218	20	10.47 ± 0.54	12.59 ± 0.89	0.85 ± 0.07	32.55	13.54	25	0.99	5.58	0.71
218	30	11.36 ± 0.58	11.83 ± 0.81	0.98 ± 0.08	32.55	12.72	25	0.99	5.58	0.71
218	50	11.39 ± 0.58	12.58 ± 0.86	0.92 ± 0.08	32.98	13.35	50	0.93	6.93	0.52
222	5	10.59 ± 0.55	10.00 ± 0.84	1.08 ± 0.11	30.57	11.45	2	0.57	0.37	0.62
222	10	11.37 ± 0.59	10.40 ± 0.86	1.11 ± 0.11	30.79	11.82	10	0.55	0.54	0.57
222	20	11.33 ± 0.59	9.11 ± 0.85	1.27 ± 0.14	31.96	9.98	25	0.42	1.15	0.33
222	30	8.88 ± 0.46	9.16 ± 0.84	0.99 ± 0.10	31.96	10.03	25	0.42	1.15	0.33
222	50	9.95 ± 0.52	9.45 ± 0.93	1.07 ± 0.12	32.92	10.05	50	0.70	5.24	0.36
227	2	8.85 ± 0.45	9.65 ± 0.85	0.93 ± 0.10	30.72	10.99	2	0.36	0.37	0.32
227	10	9.66 ± 0.50	9.32 ± 0.83	1.06 ± 0.11	30.77	10.60	10	0.34	0.31	0.30
227	20	9.72 ± 0.51	9.15 ± 0.86	1.08 ± 0.12	32.15	9.96	25	0.45	2.07	0.30
227	30	9.09 ± 0.47	9.53 ± 0.85	0.97 ± 0.10	32.15	10.37	25	0.45	2.07	0.30
230	2	10.98 ± 0.57	10.71 ± 0.91	1.04 ± 0.10	28.96	12.94	2	0.68	0.04	0.80
230	5	11.69 ± 0.60	9.92 ± 0.82	1.20 ± 0.12	28.96	11.99	2	0.68	0.04	0.80
230	20	10.73 ± 0.56	10.70 ± 0.86	1.02 ± 0.10	29.89	12.53	25	0.67	0.06	0.79
230	30	11.24 ± 0.58	10.99 ± 0.86	1.04 ± 0.10	30.54	12.59	35	0.84	1.77	0.86
230	50	11.23 ± 0.58	12.07 ± 0.89	0.95 ± 0.09	31.70	13.33	50	1.41	7.60	1.07
235	2	10.16 ± 0.52	9.83 ± 0.81	1.05 ± 0.10	28.89	11.91	2	0.62	0.12	0.72
235	5	10.23 ± 0.53	8.81 ± 0.82	1.18 ± 0.13	28.89	10.67	2	0.62	0.12	0.72
235	20	10.92 ± 0.56	9.05 ± 0.82	1.23 ± 0.13	29.71	10.66	25	0.66	0.08	0.77
235	30	8.35 ± 0.43	9.83 ± 0.84	0.87 ± 0.09	29.71	11.58	25	0.66	0.08	0.77
235	50	10.55 ± 0.54	9.75 ± 0.83	1.10 ± 0.11	31.04	10.99	52	0.96	3.44	0.87
239	2	9.97 ± 0.52	10.05 ± 0.85	1.01 ± 0.10	28.53	12.33	2	0.48	0.14	0.51
239	10	10.12 ± 0.53	10.34 ± 0.83	1.00 ± 0.09	28.73	12.60	10	0.46	0.22	0.48
239	20	9.08 ± 0.47	10.26 ± 0.81	0.90 ± 0.08	31.04	11.57	28	0.26	0.61	0.16
239	50	10.36 ± 0.54	9.90 ± 0.84	1.07 ± 0.11	32.08	10.80	50	0.97	6.90	0.56

245	2	7.92	±	0.42	8.85	±	0.81	0.91	±	0.10	29.32	10.56	2	0.20	0.34	0.09
245	4	8.35	±	0.44	8.76	±	0.84	0.97	±	0.11	29.32	10.45	2	0.20	0.34	0.09
245	20	9.50	±	0.49	7.48	±	0.81	1.29	±	0.15	30.49	8.58	18	0.26	1.31	0.10
245	30	8.19	±	0.42	8.54	±	0.85	0.98	±	0.11	32.45	9.22				0.00
245	50	8.63	±	0.45	8.71	±	0.83	1.01	±	0.11	32.45	9.39	50	0.46	4.37	0.11
250	4	7.94	±	0.42	7.89	±	0.82	1.02	±	0.12	29.74	9.28	2	0.20	0.10	0.11
250	10	7.05	±	0.38	6.78	±	0.82	1.06	±	0.14	29.74	7.98	10	0.24	1.06	0.09
250	20	7.15	±	0.38	7.55	±	0.81	0.96	±	0.12	31.11	8.50	25	0.26	1.40	0.09
250	50	8.05	±	0.42	7.63	±	0.83	1.07	±	0.13	32.59	8.19	50	0.35	2.91	0.08
257	2	7.30	±	0.38	8.22	±	0.84	0.90	±	0.10	30.47	9.45	2	0.14	0.10	0.03
257	4	7.57	±	0.39	7.60	±	0.79	1.01	±	0.12	30.47	8.72	2	0.14	0.10	0.03
257	10	7.26	±	0.39	7.25	±	0.83	1.02	±	0.13	30.47	8.33	10	0.19	0.64	0.05
257	30	8.01	±	0.43	8.73	±	0.80	0.93	±	0.10	32.51	9.39	25	0.32	2.42	0.09
257	50	9.46	±	0.50	8.40	±	0.84	1.15	±	0.13	33.29	8.83	50	0.45	4.60	0.08
271	2	6.45	±	0.35	7.02	±	0.81	0.94	±	0.12	31.66	7.76	2	0.15	0.22	0.03
271	5	7.70	±	0.42	7.82	±	0.83	1.00	±	0.12	31.66	8.65	2	0.15	0.22	0.03
271	10	7.95	±	0.42	7.16	±	0.82	1.13	±	0.14	31.65	7.91	10	0.15	0.33	0.02
271	20	6.67	±	0.35	8.25	±	0.79	0.82	±	0.09	33.28	8.67	25	0.33	2.88	0.05
271	30	8.07	±	0.42	9.03	±	0.84	0.91	±	0.10	33.28	9.50	25	0.33	2.88	0.05
271	50	8.69	±	0.46	7.95	±	0.81	1.11	±	0.13	33.80	8.23	50	0.44	5.14	0.02
273	2	6.04	±	0.32	8.09	±	0.84	0.76	±	0.09	31.16	9.08	2	0.14	0.20	0.02
273	5	6.45	±	0.34	7.63	±	0.81	0.86	±	0.10	31.16	8.57	2	0.14	0.20	0.02
273	10	6.27	±	0.33	7.76	±	0.83	0.82	±	0.10	31.22	8.70	10	0.18	1.00	0.00
273	20	8.02	±	0.42	7.84	±	0.81	1.04	±	0.12	31.61	8.68	20	0.19	1.19	0.00
273	30	7.56	±	0.39	7.18	±	0.89	1.07	±	0.14	32.50	7.73				0.00
273	50	7.60	±	0.40	8.83	±	0.88	0.88	±	0.10	33.85	9.12	50	0.40	5.02	-0.02
276	2	4.71	±	0.26	7.91	±	0.81	0.61	±	0.07	30.84	8.98	3	0.17	0.30	0.05
276	5	4.69	±	0.26	7.95	±	0.77	0.60	±	0.07	30.84	9.02	3	0.17	0.30	0.05
276	10	5.55	±	0.29	8.40	±	0.83	0.67	±	0.08	30.87	9.53	10	0.18	0.30	0.06
276	20	7.67	±	0.40	7.11	±	0.83	1.10	±	0.14	33.05	7.53	25	0.33	3.23	0.03
276	30	8.87	±	0.47	7.84	±	0.81	1.15	±	0.13	33.05	8.30	25	0.33	3.23	0.03
276	50	7.97	±	0.42	9.00	±	0.84	0.90	±	0.10	33.89	9.29	50	0.41	4.94	0.00
280	2	4.43	±	0.24	7.60	±	0.81	0.59	±	0.07	30.56	8.70	4	0.19	0.17	0.09
280	5	4.99	±	0.26	7.66	±	0.83	0.66	±	0.08	30.56	8.77	4	0.19	0.17	0.09
280	10	5.19	±	0.28	8.84	±	0.85	0.60	±	0.07	30.59	10.11	10	0.21	0.57	0.08
280	20	7.40	±	0.39	7.89	±	0.82	0.95	±	0.11	33.07	8.35	25	0.33	2.91	0.06
280	30	7.27	±	0.38	8.46	±	0.83	0.88	±	0.10	33.07	8.96	25	0.33	2.91	0.06
280	50	7.81	±	0.40	8.69	±	0.84	0.91	±	0.10	33.74	9.01	50	0.37	3.91	0.03
285	2	4.87	±	0.26	7.29	±	0.82	0.68	±	0.08	30.52	8.35	4	0.18	0.09	0.09
285	5	4.51	±	0.24	8.76	±	0.84	0.52	±	0.06	30.52	10.04	4	0.18	0.09	0.09
285	10	5.00	±	0.27	8.80	±	0.84	0.58	±	0.06	30.54	10.09	10	0.16	0.08	0.06
285	20	7.17	±	0.38	8.64	±	0.82	0.84	±	0.09	33.05	9.15	25	0.37	3.22	0.08
285	30	7.14	±	0.37	8.84	±	0.84	0.82	±	0.09	33.05	9.36	25	0.37	3.22	0.08
285	50	7.55	±	0.39	8.98	±	0.84	0.86	±	0.09	34.08	9.22	50	0.47	5.79	0.01

*) normalized to the average activity ratio at depths>MLD at ice stations.

**) fraction of Pacific Water derived from nutrient data according to Jones et al. (1998)

Figure legends

Fig. 1. Cruise track of expedition ARK XXVI/3 superimposed on AMRSR-2 sea ice concentration (http://www.meereisportal.de) at the time of the first (left) and last (right) ice station.

Fig. 2. Mixed Layer Depth along the cruise track, estimated according to the definition of Shaw et al. (2009).

Fig. 3. a) Salinity, b) potential temperature and c) potential density anomaly in the upper 60m layer of five stations on a transect across the ice edge from ice-covered Sta 271 (green diamonds) and 272 (blue dots) through ice edge station 273 (magenta circles) to open water stations 274 (black pentagons) and 276 (red crosses).

Fig. 4. ^{226}Ra (dpm/100L) normalized to salinity 35 as function of left, Pacific water fraction f_P, with corresponding regression line $^{226}Ra_{35} = 8.83 + 4.54\ f_P$ ($R^2 = 0.73$), and right, depth, identifying the stations with f_P>0.2: Sta 212 (filled squares), 218 (filled diamonds), 222 (triangles), 227 (crosses), 230 (filled circles), 235 (open squares), and 239 (open circles).

Fig. 5. Left, $^{222}Rn/^{226}Ra$ ratio for all stations with full ice cover with profile of means with 95% CI (n= 10,11,9,11,11,12 for 2,5,10,20,30, and 50m depth, respectively), and right, $^{222}Rn/^{226}Ra$ ratio for all stations in open water (red symbols, open diamonds, 273; circles, 276; triangles,

280; squares, 285) compared with mean and 95% CI at ice-covered stations from left panel. The estimated standard error in activity ratio for the individual data points is 11%.

Fig. 6. Air temperature (heavy line) compared to freezing temperature of surface water (broken line) and wind speed (thin line) while the ship was in the ice.

Fig. 7. Average (with 95% CI) of ^{222}Rn concentration profiles at six ice stations (212, 218, 222, 227, 230, 235) sampled under an ice floe (closed symbols) and from the ship (open symbols).

Fig. 8. Average ^{222}Rn/^{226}Ra ratio in the upper 20m of the water column compared to equilibrium (full line) and weighted fraction sea ice cover (open circles) (left) and corresponding gas transfer velocity using eq. (4) (right). Error bars represent one standard deviation. Broken lines indicate 95% CI for the average values for ice covered (201-271) and open water (276, 280, 285) stations.

Fig. 9. gas transfer velocity in open water stations derived from eq. (4) using the radon depletion in the upper 21m compared with the relationships given by Wanninkhof (1992, full line) and by Ho et al. (2011, broken line) as function of the wind speed from wind reanalysis weighted according to ^{222}Rn decay and ML flushing (wt2 in Table 2). Sta 273 is closest to the ice edge.

Fig. 10. Left, development of ice cover around Sta 250 to 276 (polar projection with 120°E meridian indicated) during the last 18 days the ship was in the ice and right, development of

ice cover around Sta 257, 271 and 273 during the last 6 days before sampling (scale: pixels are 6x6km) with 9-pixel block (black square) around sampling location (red dot) used to derive ice cover history.

Fig. 11. Wind bearing vector (to where wind is blowing, in m/s) in 8 days preceding sampling at all four open water stations, showing the predominantly southerly winds just before sampling of Sta 273. Dot is wind vector at day of sampling according to wind reanalysis.

Fig. 12. Distribution of potential density anomaly (kg m^{-3}) on the N-S section of Sta 271-276 including intermediate XCTD casts, with enhanced colour contrast at the base of the surface layer showing deep penetration of surface water near the ice edge (Sta 273).

Fig. 13. Gas transfer velocity at all stations from radon depletion (filled circles, with SE and for ice covered stations (201-271) and open water stations (276-285) the 95% CI for the average values indicated by broken lines as in Fig. 6) compared with the value expected from wind reanalysis, weighting and the relationship of Wanninkhof (1992) without scaling for the fraction open water.

Fig. 14 left- Gas transfer velocity (with SD) at all stations from radon depletion versus the velocity expected from wind reanalysis, weighting, and the relationship of Wanninkhof (1992) assuming a linear scaling with the open water fraction according to Takahashi et al., (2009), right- Gas transfer efficiency (with SD) as function of the weighted fraction of open water, compared with the relationship expected if gas transfer scaled linearly with ice cover (dashed lines represent 1:1 slope, negative values of k or E_T have no physical meaning).

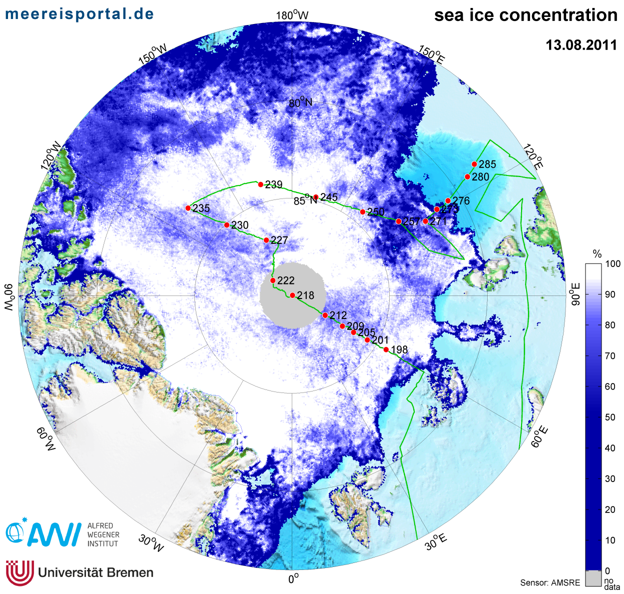

meereisportal.de
sea ice concentration
13.08.2011
180°W
150°W
150°E
120°W
120°E
80°N
85°N
90°W
90°E
60°W
60°E
30°W
30°E
0°
285
280
276
273
271
257
250
245
239
235
230
227
222
218
212
209
205
201
198
%
100
90
80
70
60
50
40
30
20
10
0
no data
Sensor: AMSRE
ALFRED WEGENER INSTITUT
Universität Bremen

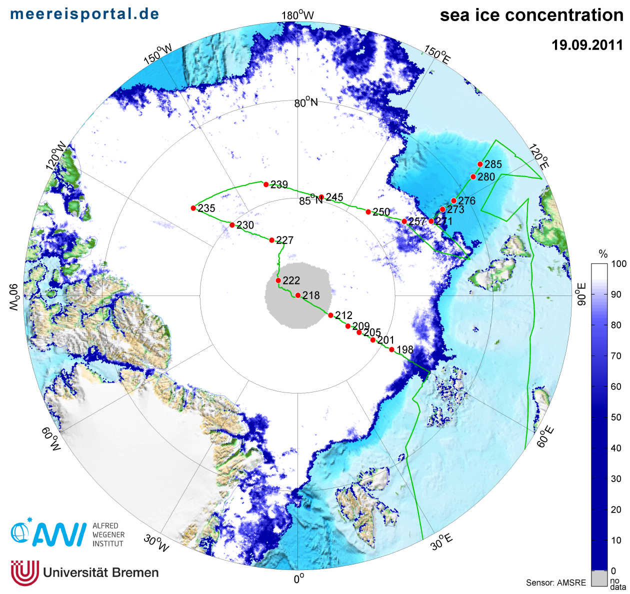

meereisportal.de
sea ice concentration
19.09.2011
180°W
150°W
150°E
120°W
120°E
80°N
85°N
90°W
90°E
60°W
60°E
30°W
30°E
0°
285
280
276
273
271
257
250
245
239
235
230
227
222
218
212
209
205
201
198
%
100
90
80
70
60
50
40
30
20
10
0
no data
Sensor: AMSRE
ALFRED WEGENER INSTITUT
Universität Bremen

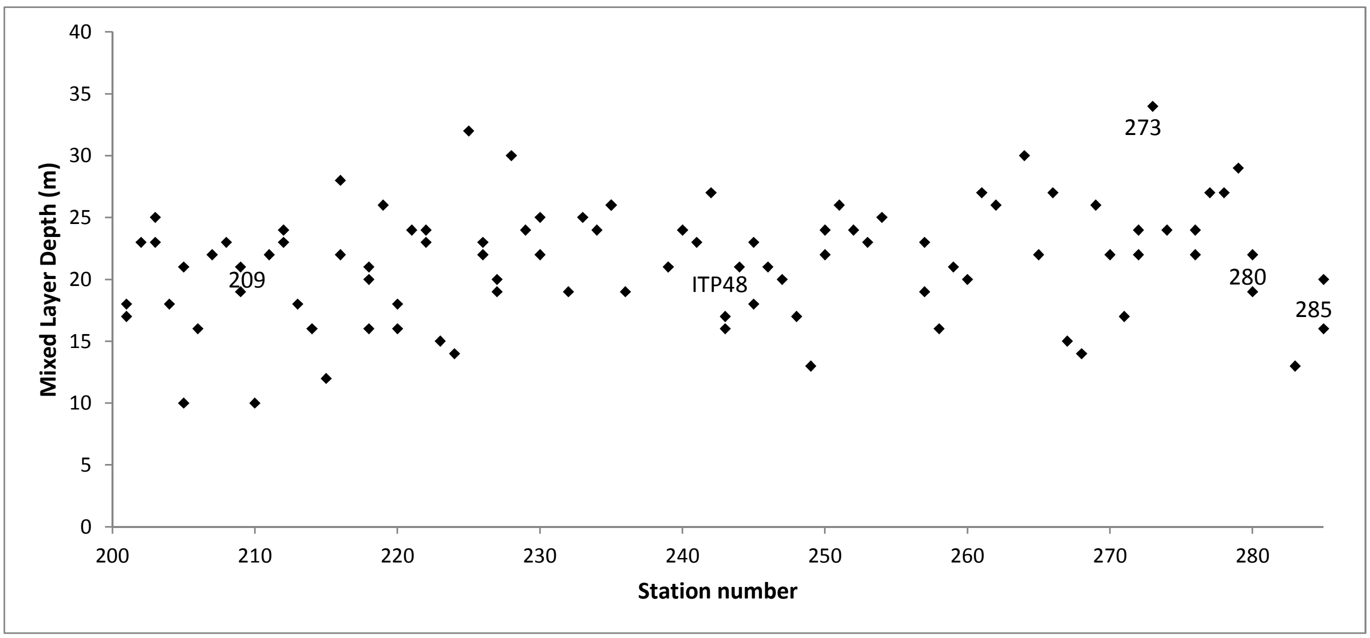

Mixed Layer Depth (m)
Station number
209
ITP48
273
280
285
0
5
10
15
20
25
30
35
40
200
210
220
230
240
250
260
270
280

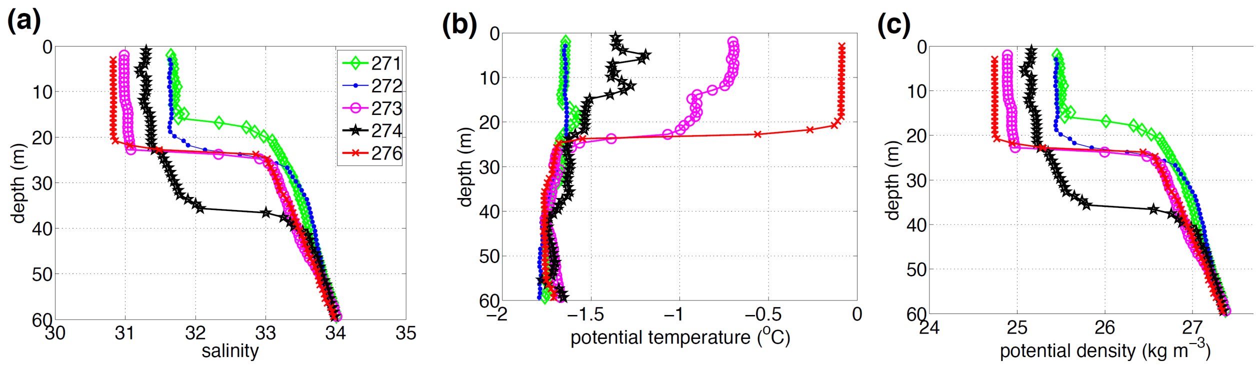
(a)
(b)
(c)
depth (m)
salinity
potential temperature (°C)
potential density (kg m−3)
271
272
273
274
276

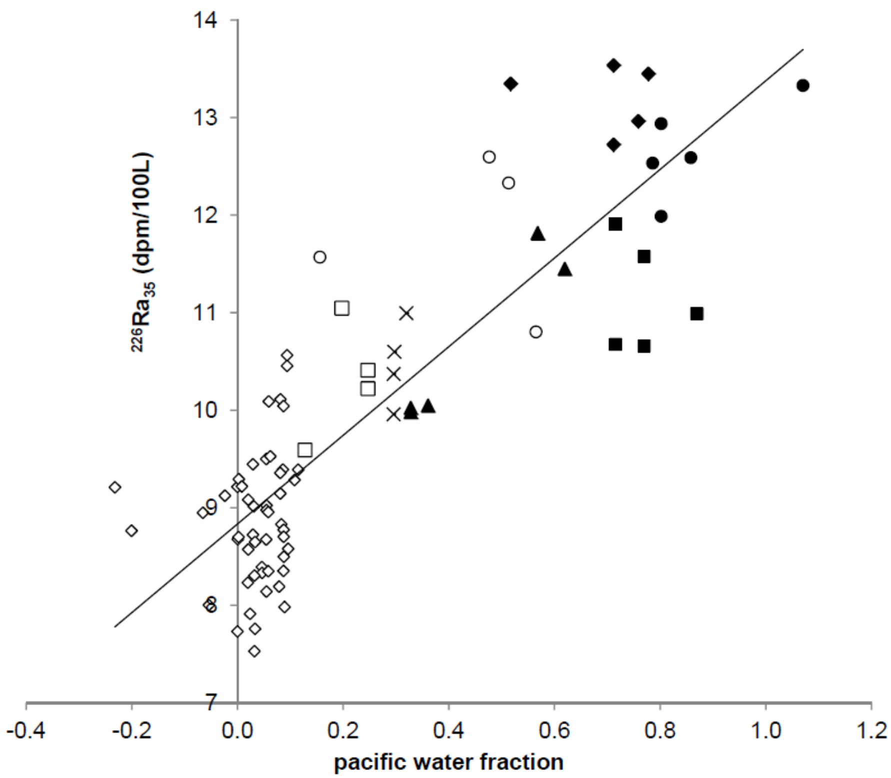

$^{226}Ra_{35}$ (dpm/100L)
pacific water fraction

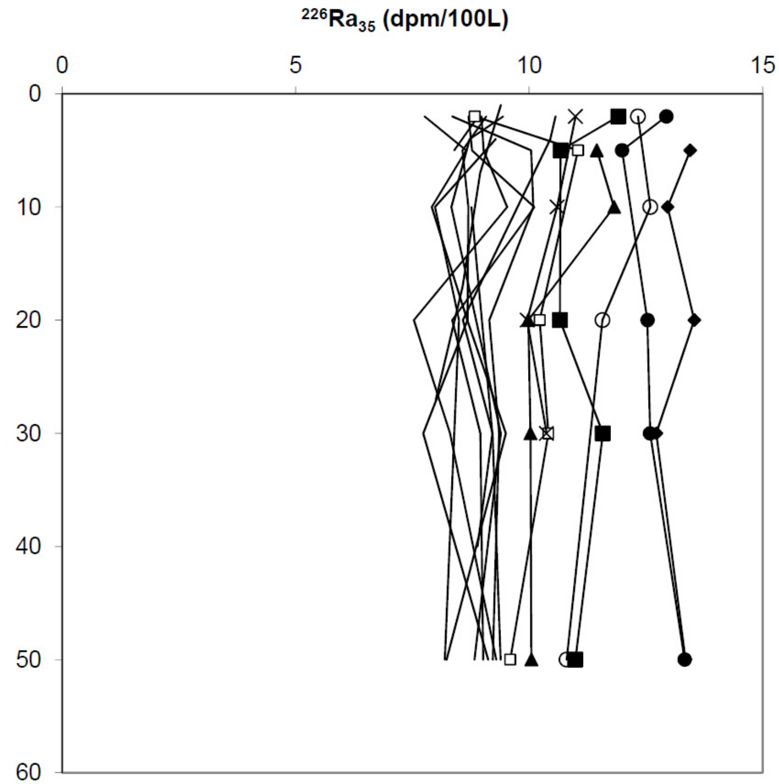

$^{226}Ra_{35}$ (dpm/100L)

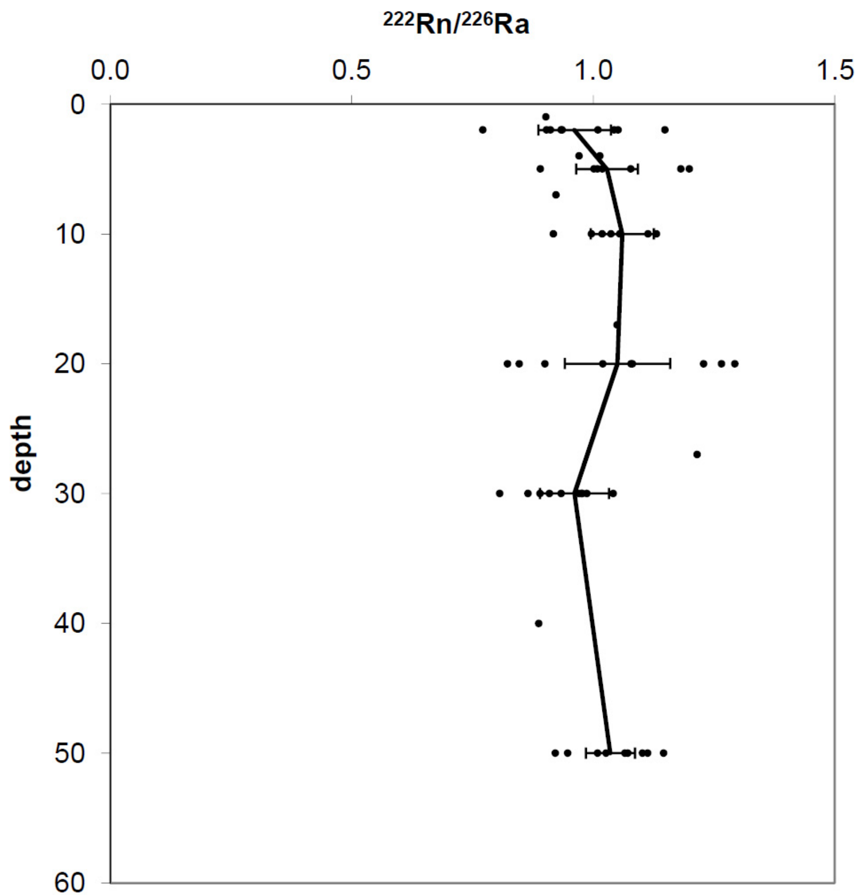

$^{222}Rn/^{226}Ra$
0.0
0.5
1.0
1.5
0
10
20
30
40
50
60
depth

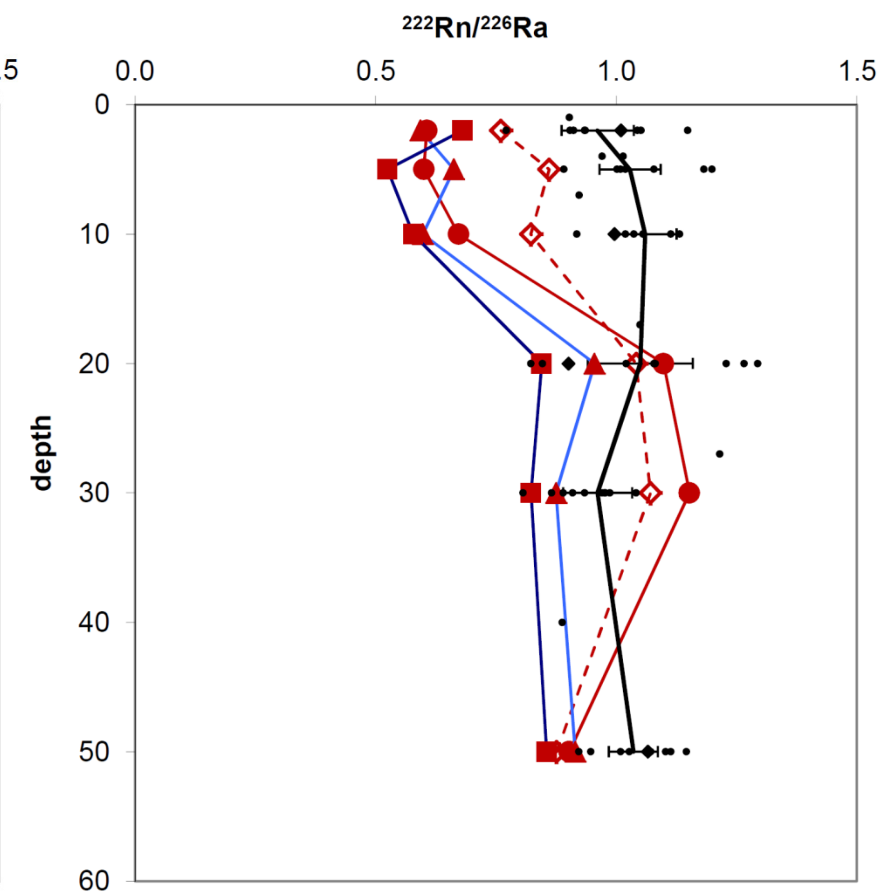

$^{222}Rn/^{226}Ra$
0.0
0.5
1.0
1.5
0
10
20
30
40
50
60
depth

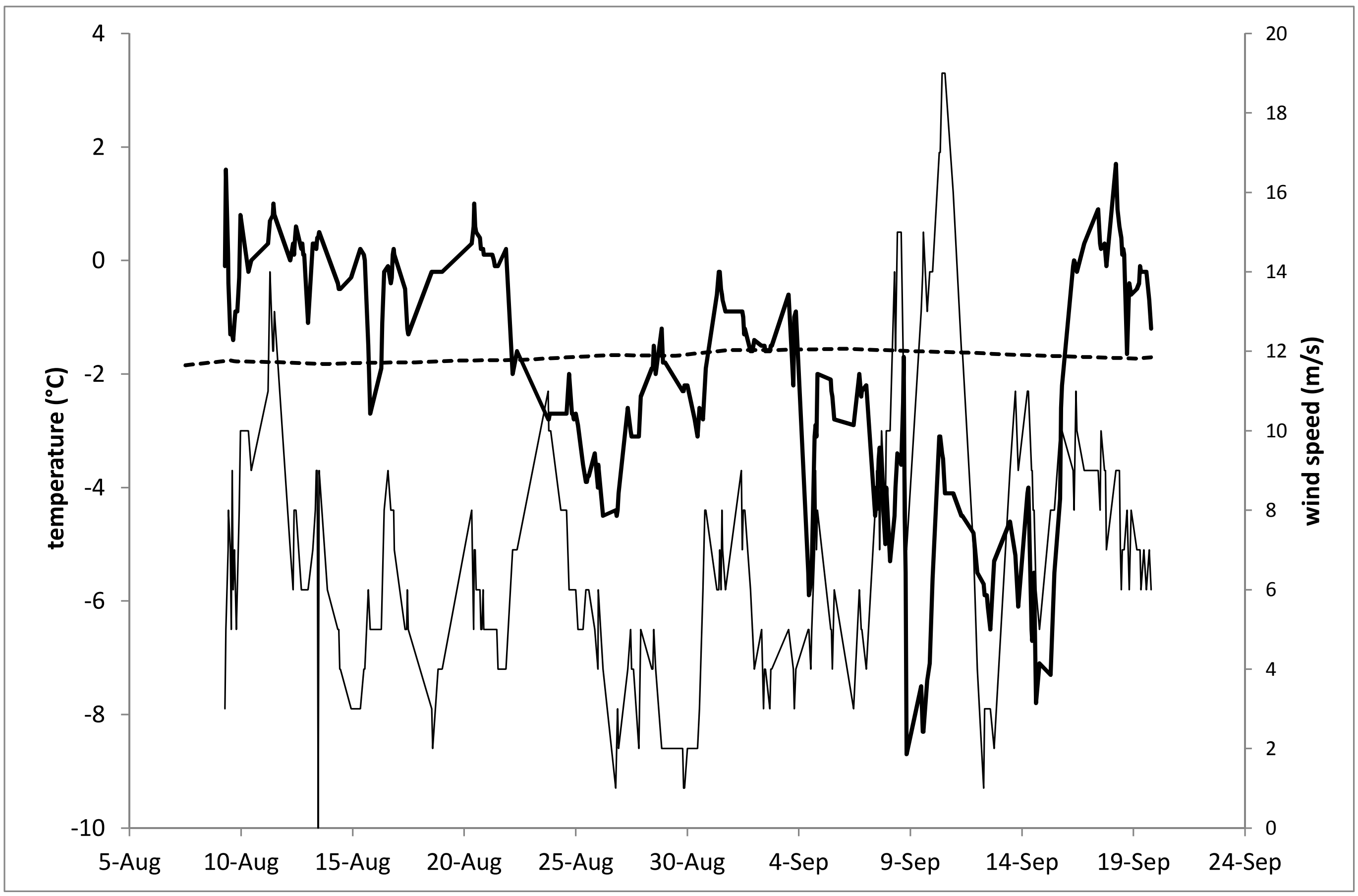

4
2
0
-2
-4
-6
-8
-10
temperature (°C)
20
18
16
14
12
10
8
6
4
2
0
wind speed (m/s)
5-Aug
10-Aug
15-Aug
20-Aug
25-Aug
30-Aug
4-Sep
9-Sep
14-Sep
19-Sep
24-Sep

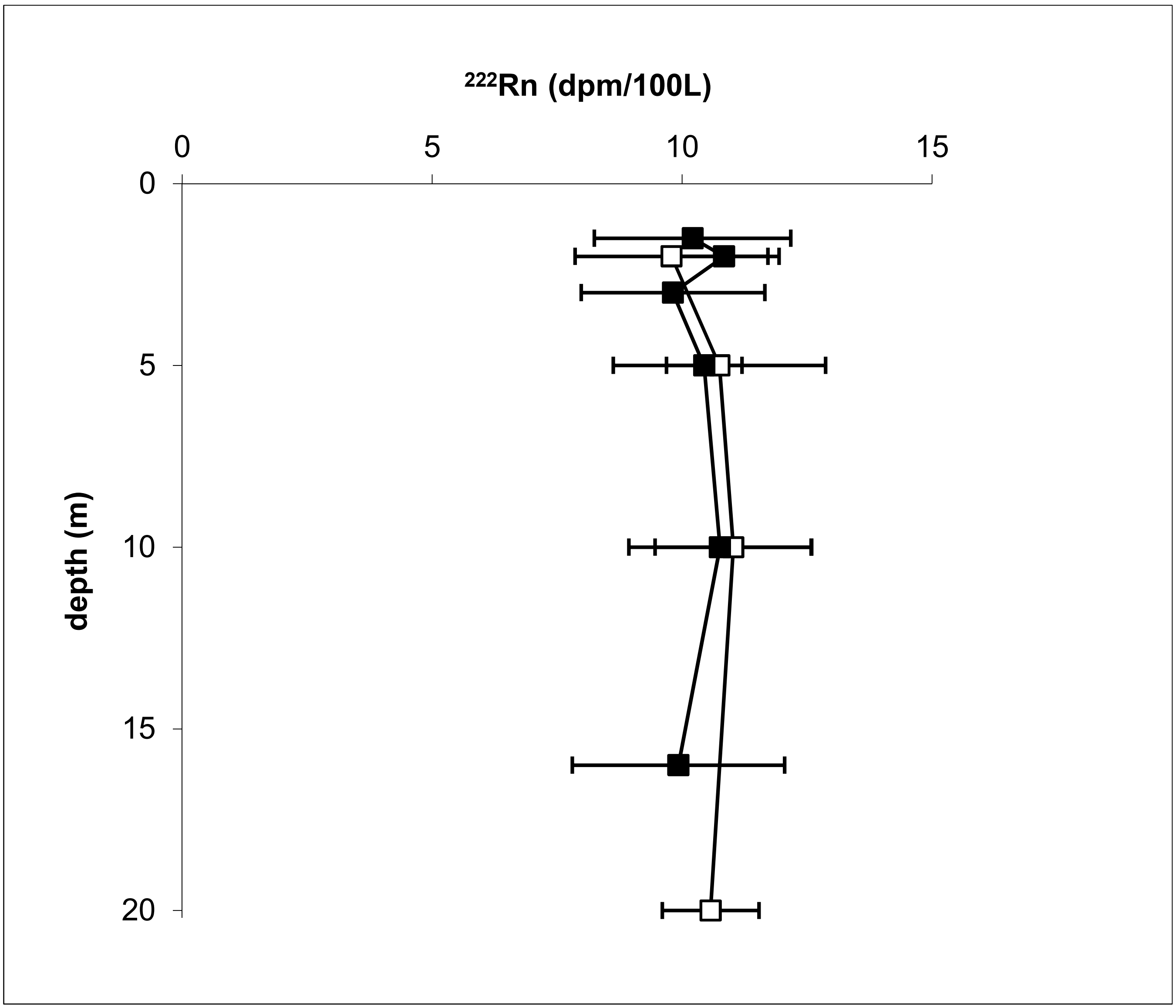

^{222}Rn (dpm/100L)
0
5
10
15
0
5
10
15
20
depth (m)

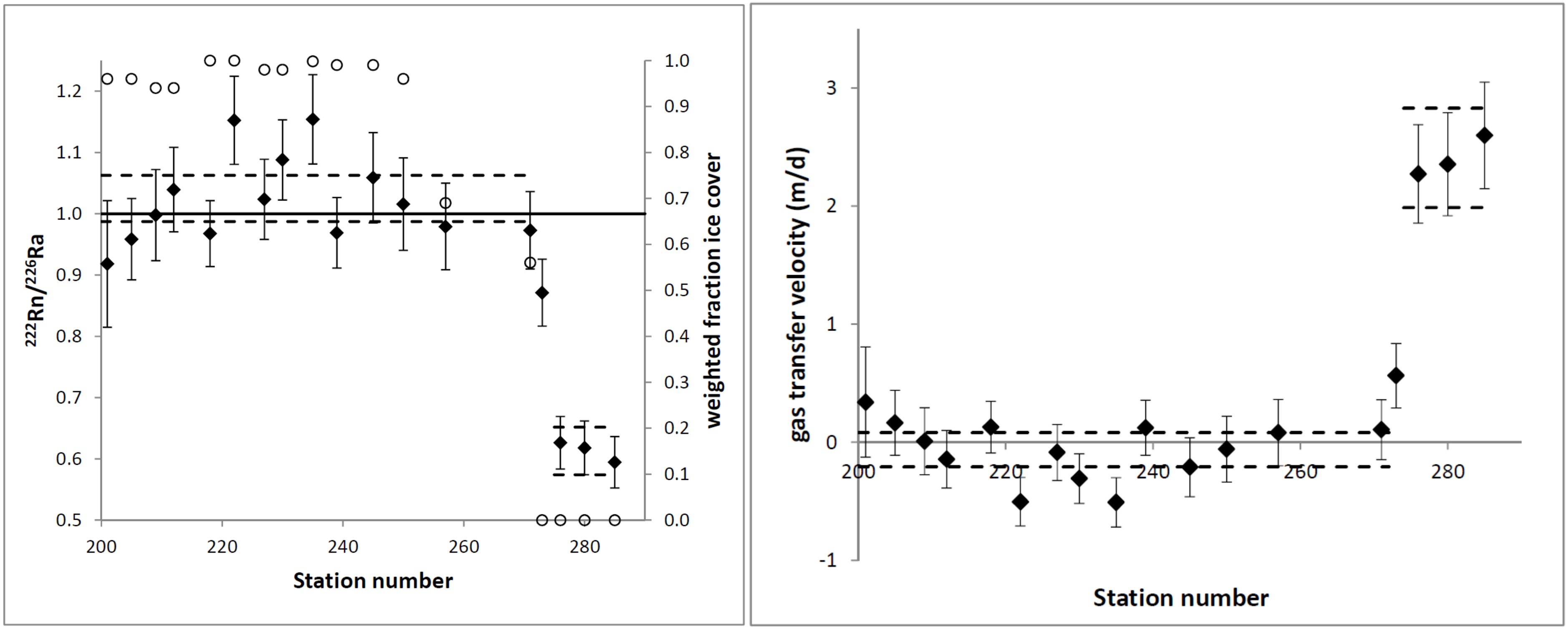

$^{222}Rn/^{226}Ra$
weighted fraction ice cover
Station number
gas transfer velocity (m/d)
Station number

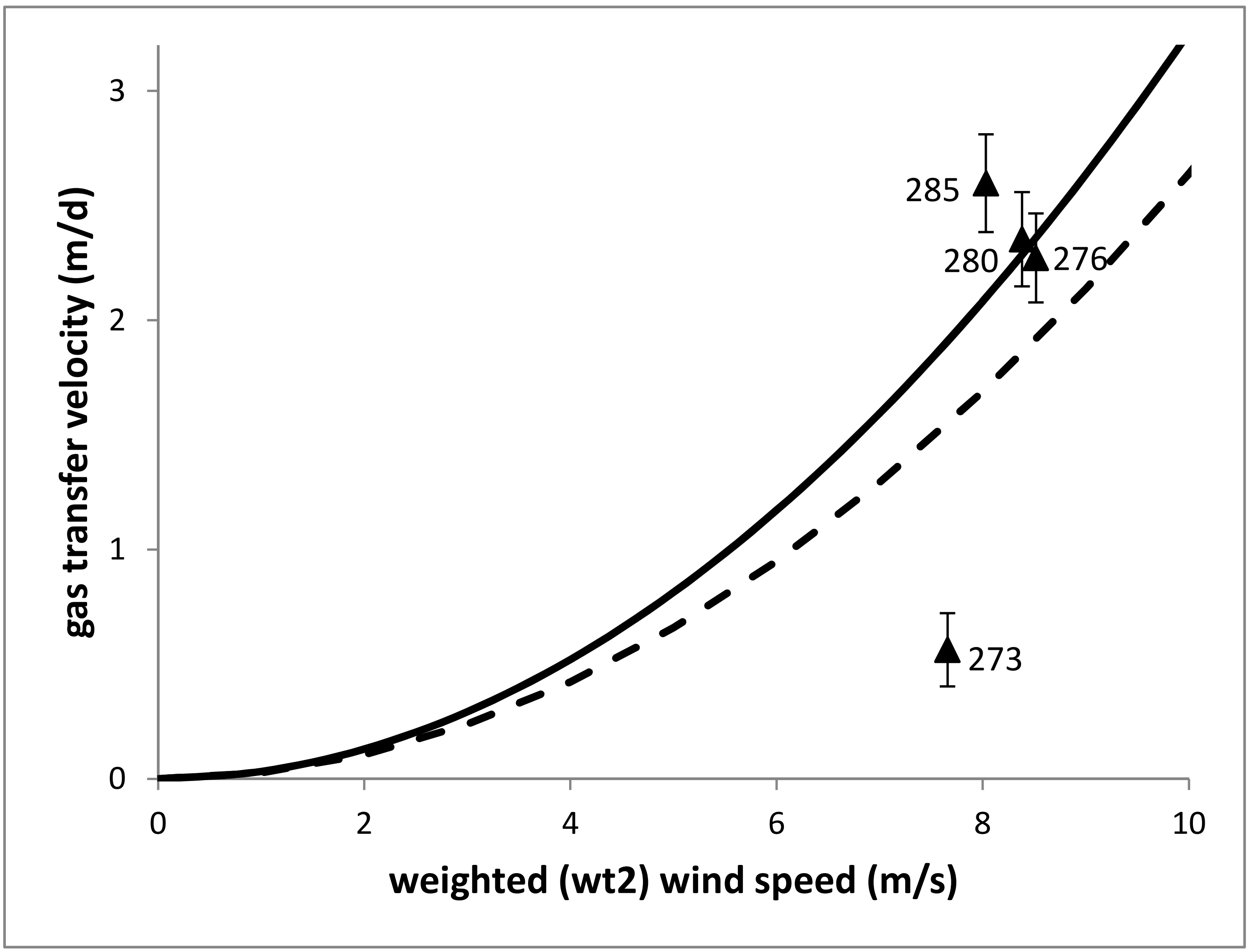

gas transfer velocity (m/d)
weighted (wt2) wind speed (m/s)
0
1
2
3
0
2
4
6
8
10
285
280
276
273

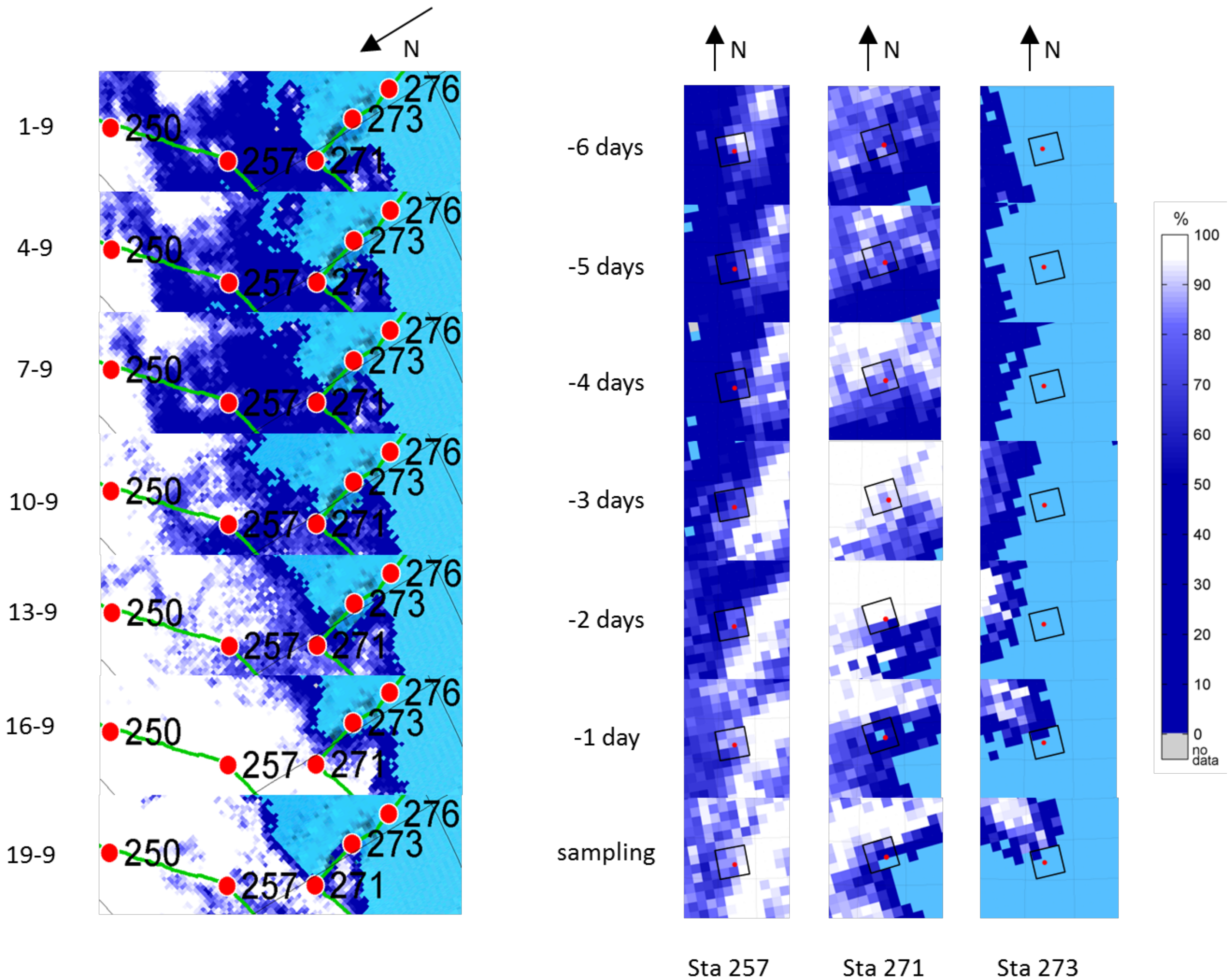
N
1-9
4-9
7-9
10-9
13-9
16-9
19-9
250
257
271
273
276
-6 days
-5 days
-4 days
-3 days
-2 days
-1 day
sampling
Sta 257
Sta 271
Sta 273
%
100
90
80
70
60
50
40
30
20
10
0
no data


273
17-9
12-9
19-9
276
18-9
20-9
12-9
280
18-9
13-9
21-9
285
N
18-9
W
E
21-9
22-9
15-9
S

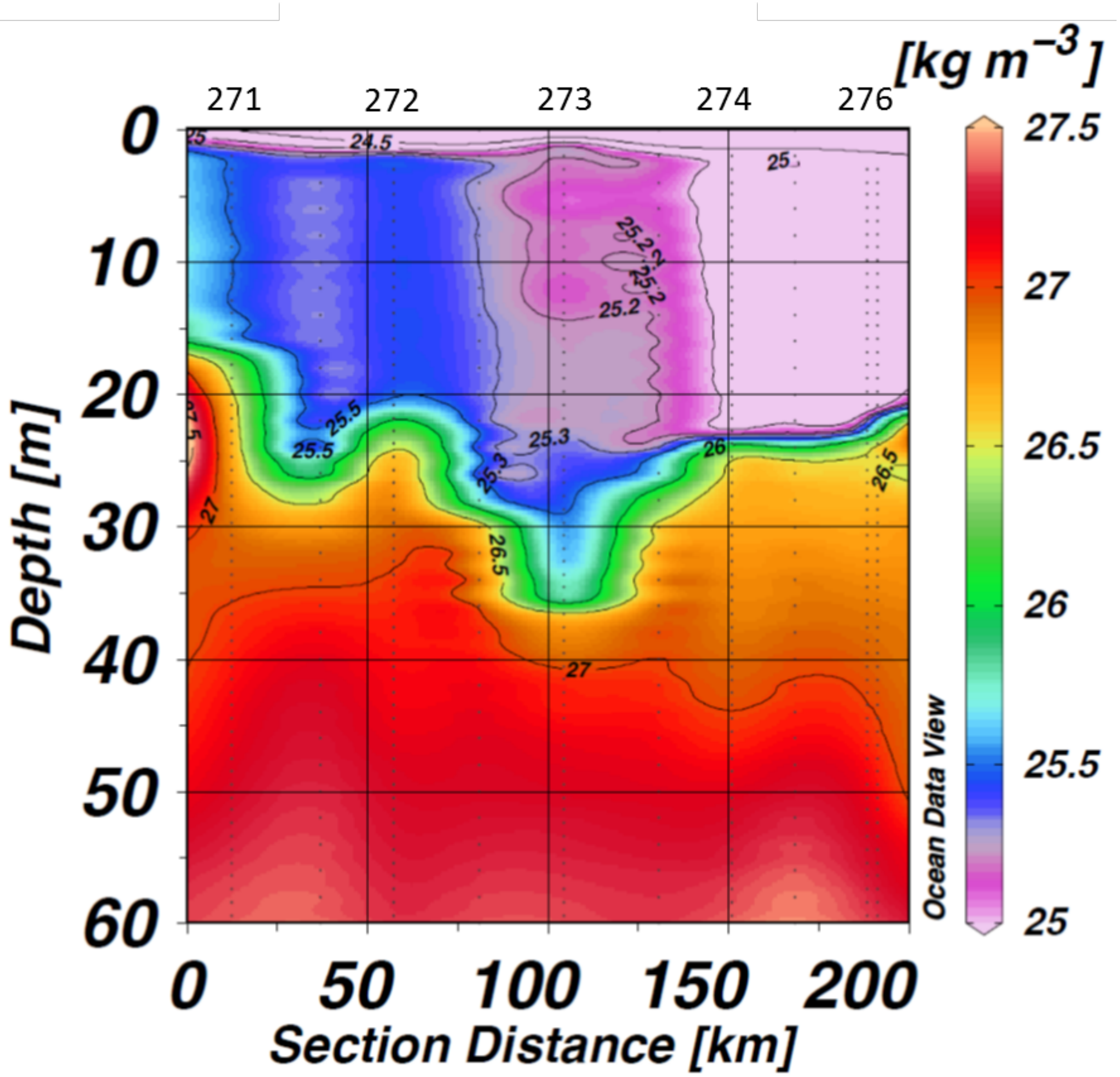

[kg m⁻³]
271
272
273
274
276
0
10
20
30
40
50
60
Depth [m]
0
50
100
150
200
Section Distance [km]
27.5
27
26.5
26
25.5
25
Ocean Data View
24.5
25.2
25.3
25.5
26.5

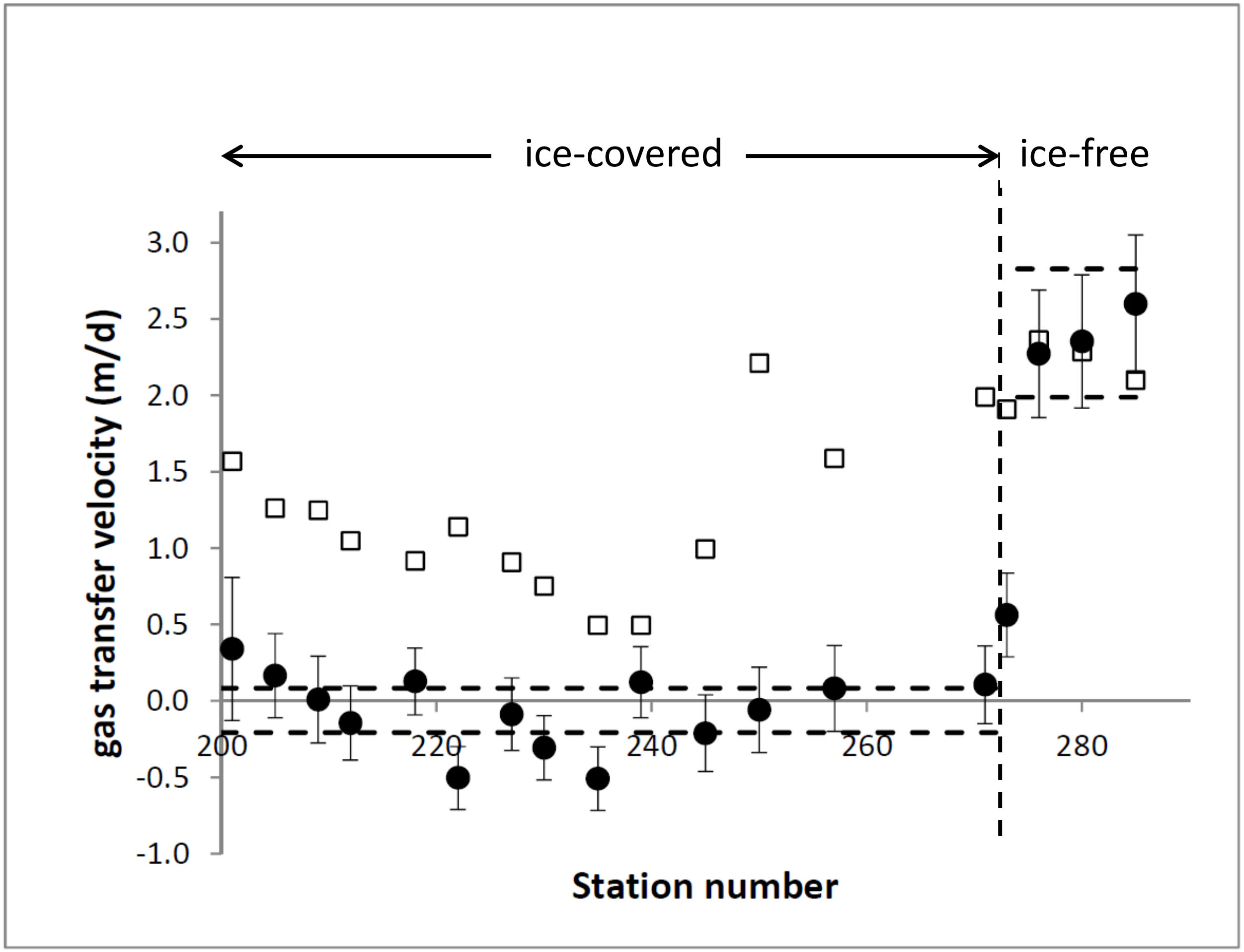
ice-covered
ice-free
gas transfer velocity (m/d)
3.0
2.5
2.0
1.5
1.0
0.5
0.0
-0.5
-1.0
200
220
240
260
280
Station number

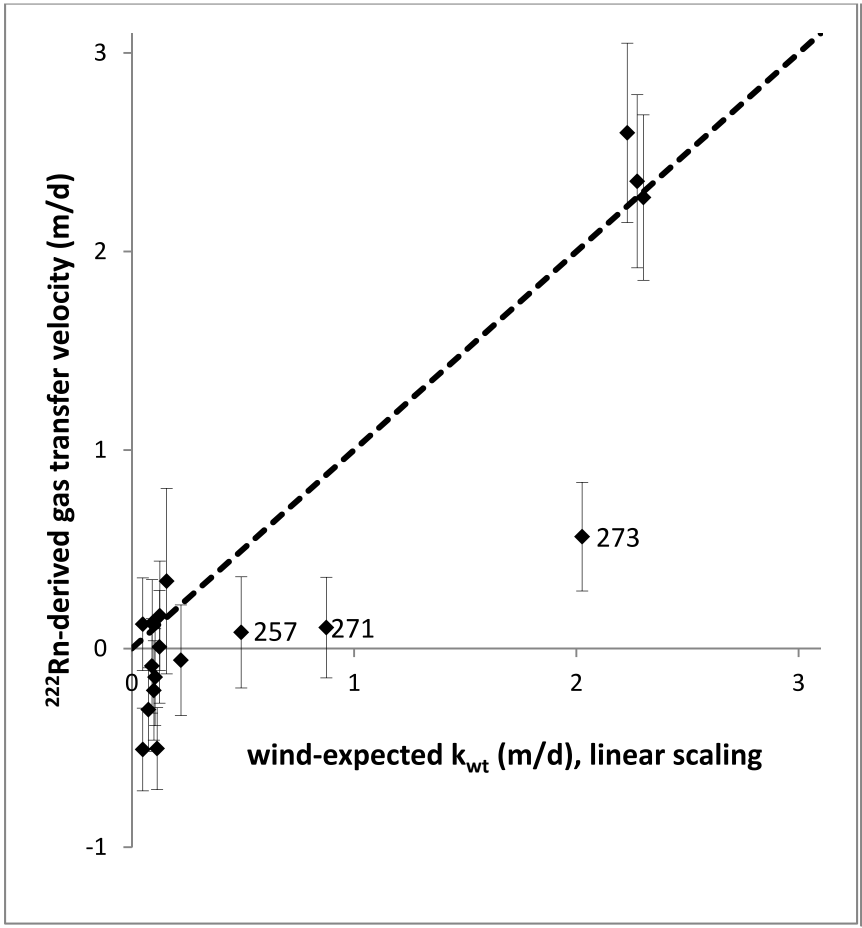

^{222}Rn-derived gas transfer velocity (m/d)
wind-expected k_{wt} (m/d), linear scaling
257
271
273
3
2
1
0
-1
0
1
2
3

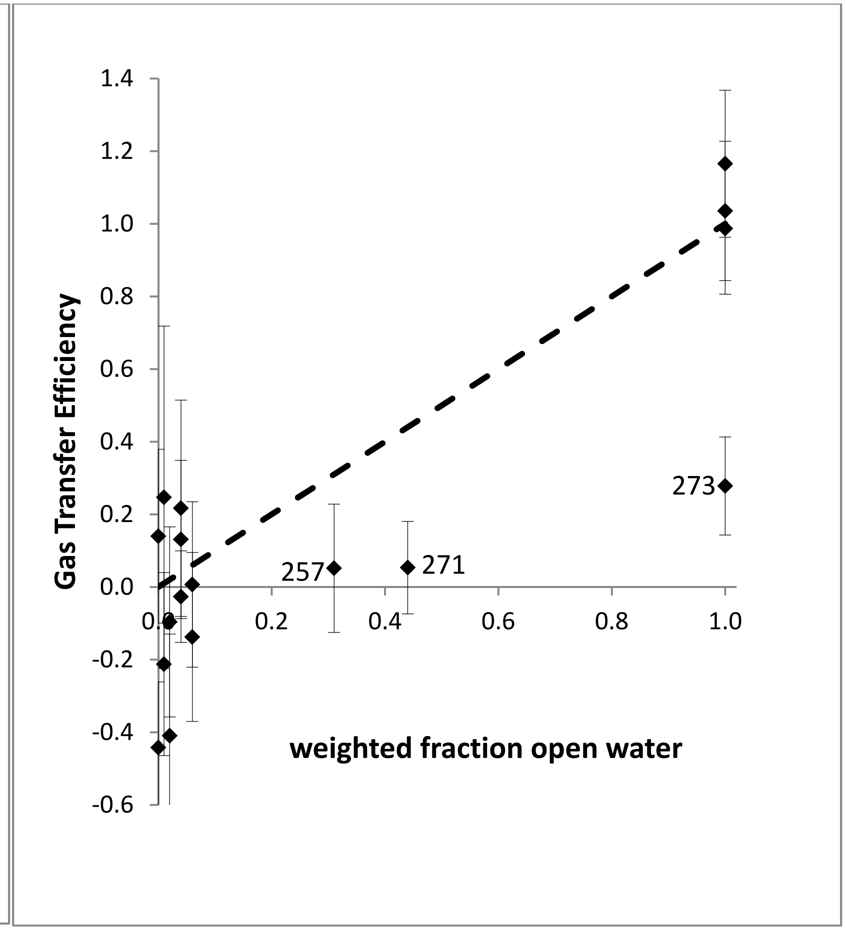

Gas Transfer Efficiency
weighted fraction open water
257
271
273
1.4
1.2
1.0
0.8
0.6
0.4
0.2
0.0
-0.2
-0.4
-0.6
0.2
0.4
0.6
0.8
1.0